2014

Using Micro-Gravity Techniques to Map Alluvium Thickness and Pleistocene Location of the West Branch of the Susquehanna River Near Muncy, Pennsylvania

Matthew Joseph Sirianni
Bucknell University, mjs081@bucknell.edu

USING MICRO-GRAVITY TECHNIQUES TO MAP ALLUVIUM THICKNESS AND PLEISTOCENE LOCATION OF THE WEST BRANCH OF THE SUSQUEHANNA RIVER NEAR MUNCY, PENNSYLVANIA

By

Matthew J Sirianni

Thesis Submitted to the Honors Council

For Honors in Geology

9 May 2014

Approved by:

____

Advisor: Robert W. Jacob, PhD

____

Advisor: Benjamin Hayes, PhD

____

Department Chairperson: Jeffrey Trop, PhD

Acknowledgements

I would like to thank the Susquehanna River Initiative and the Environmental Center for the funding that allowed this project to happen, as well as the Geology Department for their support and funding for my travels to various conferences. I would also like to thank my advisors Dr. Jacob, and Dr. Hayes for their endless hours of work and guidance in teaching me geophysics before I had even taken the class, and their support and encouragement throughout the data collection and interpretation process. I would like to thank Dr. Salyards for participating on my Honor's Thesis Committee and providing valuable direction and ideas for improving my thesis. I would like to thank my parents and my sister for providing me endless support throughout my life and for encouraging me to pursue any and all of my academic pursuits. I would like to thank Brad Jordan for giving me access to all of the field equipment I needed, as well as Carilee Dill for coordinating all of my travel expenses and always having a full bowl of candy. I would like to thank Rene Talai for always being there for me and staying up with me on all the late nights I spent in the lab, she truly kept me sane throughout this whole process. And lastly I would like to thank all of my friends who have come out to support me at all of my campus presentations.

Table of Contents

List of Figures

Abstract

Laurentide glaciation during the early Pleistocene (~970 ka) dammed the southeast-flowing West Branch of the Susquehanna River (WBSR), scouring bedrock and creating 100-km-long glacial Lake Lesley near the Great Bend at Muncy, Pennsylvania (Ramage et al., 1998). Local drill logs and well data indicate that subsequent paleo-outwash floods and modern fluvial processes have deposited as much as 30 meters of alluvium in this area, but little is known about the valley fill architecture and the bedrock-alluvium interface. By gaining a greater understanding of the bedrock-alluvium interface the project will not only supplement existing depth to bedrock information, but also provide information pertinent to the evolution of the Muncy Valley landscape. This project determined if variations in the thickness of the valley fill were detectable using micro-gravity techniques to map the bedrock-alluvium interface. The gravity method was deemed appropriate due to scale of the study area (~30 km^2), ease of operation by a single person, and the available geophysical equipment.

A LaCoste and Romberg Gravitron unit was used to collect gravitational field readings at 49 locations over 5 transects across the Muncy Creek and Susquehanna River valleys (approximately 30 km^2), with at least two gravity base stations per transect. Precise latitude, longitude and ground surface elevation at each location were measured using an OPUS corrected Trimble RTK-GPS unit. Base stations were chosen based on ease of access due to the necessity of repeat measurements. Gravity measurement locations were selected and marked to provide easy access and repeat measurements. The

gravimeter was returned to a base station within every two hours and a looping procedure was used to determine drift and maximize confidence in the gravity measurements. A two-minute calibration reading at each station was used to minimize any tares in the data.

The Gravitron digitally recorded finite impulse response filtered gravity measurements every 20 seconds at each station. A measurement period of 15 minutes was used for each base station occupation and a minimum of 5 minutes at all other locations. Longer or multiple measurements were utilized at some sites if drift or other externalities (i.e. train or truck traffic) were effecting readings. Average, median, standard deviation and 95% confidence interval were calculated for each station. Tidal, drift, latitude, free-air, Bouguer and terrain corrections were then applied.

The results show that the gravitational field decreases as alluvium thickness increases across the axes of the Susquehanna River and Muncy Creek valleys. However, the location of the gravity low does not correspond with the present-day location of the West Branch of the Susquehanna River (WBSR), suggesting that the WBSR may have been constrained along Bald Eagle Mountain by a glacial lobe originating from the Muncy Creek Valley to the northeast. Using a 3-D inversion model, the topography of the bedrock-alluvium interface was determined over the extent of the study area using a density contrast of -0.8 g/cm^3. Our results are consistent with the bedrock geometry of the area, and provide a low-cost, non-invasive and efficient method for exploring the subsurface and for supplementing existing well data.

Background

Geomorphological History

The “Great Bend” of the West Branch of the Susquehanna River (WBSR) is located in Muncy, Pennsylvania (PA) in Lycoming County, within the Valley and Ridge Province of Central PA (**Figure 1A**).

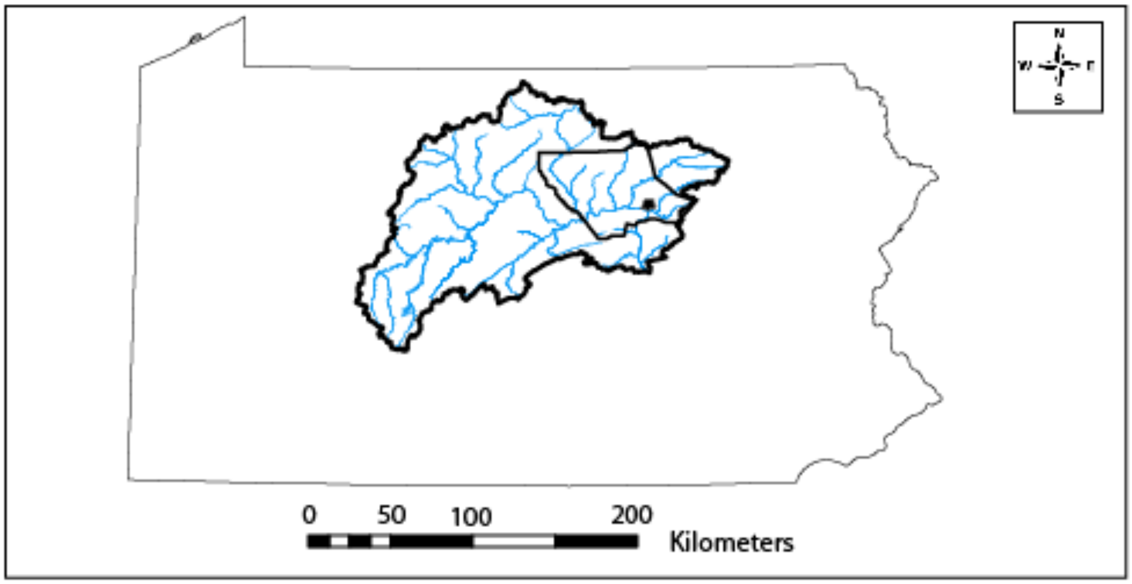

Figure 1A: Reference map showing the location of Muncy, PA in Lycoming County situated in the West Branch of the Susquehanna River watershed.

Over the past several million years, this region has been subject to multiple episodes of glaciation. The fingerprints of the subsequent debris flows and outwash floods are evident on the landscape today and in many places control the hydrology and ecology of the region (Kochel et al, 2009; Pazzaglia and Gardner, 1993; Nelson, 1965; Peltier, 1949). Geomorphic and sedimentologic evidence indicate that during the early Pleistocene (~770 and ~970 ka), Laurentide ice sheets blocked the Susquehanna River, forming a 100-m deep, 100-km long glacial lake, which extended from Williamsport, PA to Lock Haven, PA **(Figure 1B)**.

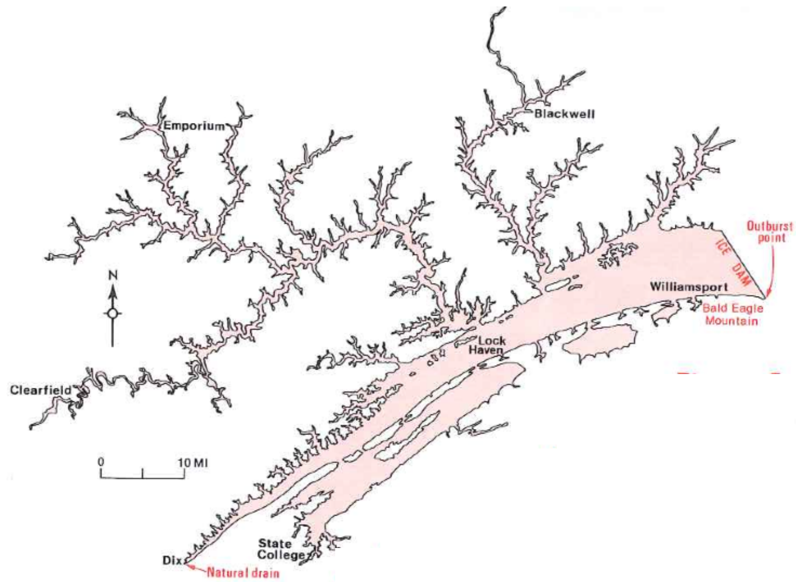

Figure 1B: Map showing the extent of Glacial Lake Lesley. Muncy, PA is located at the outburst point near Bald Eagle Mountain (Sevon, 1993).

The exact location of the glacial ice dam at the downstream end of the lake is unknown, but recent mapping of the river bedforms and valley morphology suggests it was at Muncy, where the river valley suddenly widens and deepens (Newlin and Hayes, 2013; Hayes and Newlin, 2012). One possible explanation is that a valley lobe of the continental ice sheet flowed east-west, down Muncy Creek valley and across the

Susquehanna River, forming an ice dam in the Great Bend area (Hayes, personal communication).

Study Area

The town of Muncy is positioned on the south side of the Nittany Anticline and is located directly east of the "Great Bend" of the West Branch of the Susquehanna River between the Nittany Anticline to the north and the White Deer Syncline to the south **(Figure 2)**. The bedrock throughout Muncy ranges in age from the Lower Silurian to the Upper Devonian and is dominantly shale and sandstone with the Keyser, Tonoloway and Mifflinton Formations making up the less prominent limestone bedrock present within the valley (Faill, 1979). The unconsolidated material overlying bedrock is dominantly alluvium with variable thickness while residual soils are less commonly found (Faill, 1979). The unconsolidated zone (residual soil or alluvial fill) is estimated to range between 0.5 and 30 meters and is thought to directly contact bedrock at its basal depth, but there are no basal contact exposures (Faill, 1979).

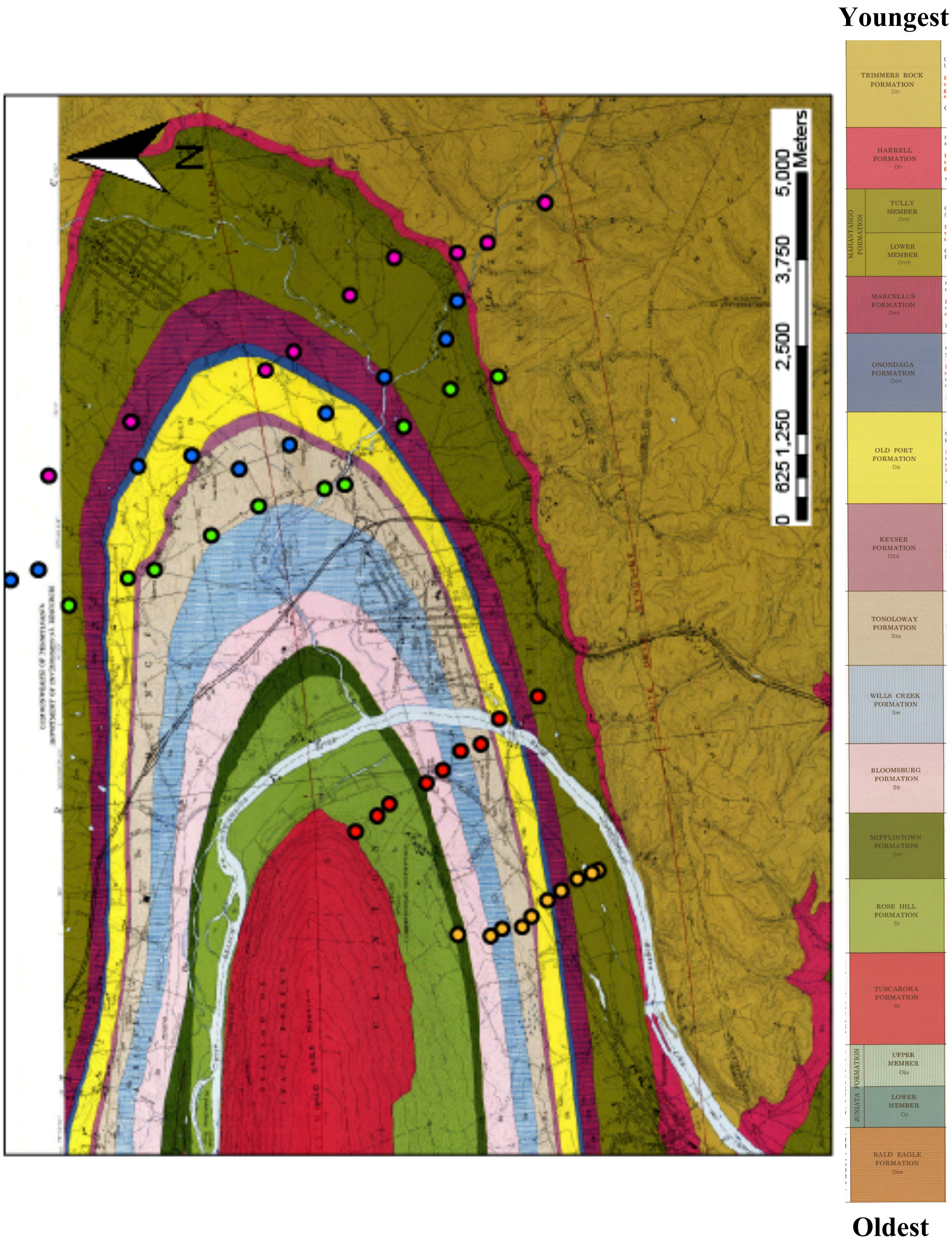

Figure 2: Bedrock geology map of Muncy, PA and surrounding area with rock unit names (Faill, 1979).

Bedrock Geology

Tuscarora Formation

The oldest unit located within the study area is the Tuscarora Formation. This formation was deposited during the Lower Silurian and is approximately 75 meters thick. This formation is a coarse grained, medium to thickly bedded quartzite with interbeds of shale and siltstones and varies in color from white to light grey to pale green to tan. The Tuscarora Formation tends to form mountains and ridges of very high relief.

Rose Hill Formation

Up-section from the Tuscarora Formation is the Rose Hill Formation. Deposited during the Middle Silurian, this shale has thick bedding with interbeds of siliceous and calcareous siltstones with colors ranging from grey to green-grey. The Rose Hill Formation tends to form low ridges with moderate relief and is 290 meters thick.

Mifflintown Formation

This finely grained dark grey limestone was deposited during the Middle Silurian. It has thin to medium bedding with interbeds of calcareous shale. The Mifflintown Formation tends to form low ridges of moderate to low relief and is 60 meters thick.

Bloomsburg Formation

The Bloomsburg Formation is a thickly bedded homogeneous red silt mudstone that was deposited during the Middle-Upper Silurian. This formation has a lower unit (interbeds of algal beds), an upper unit (interbeds of green calcareous mudstone) and is 175 meters thick.

Wills Creek Formation

The Wills Creek Formation was deposited during the Upper Silurian. The formation is characterized by thin to medium bedded mudstone and siltstones with interbedded mudstones, siltstones, limestones and dolomites. The formation forms low to moderate ridges with moderately low relief and is approximately 200-250 meters thick.

Tonoloway Formation

Deposited during the Upper Silurian, the Tonoloway Formation is a medium to dark grey laminated limestone with thin to medium bedding. This unit tends to form valleys, low relief terrain and is approximately 175-225 meters thick.

Keyser Formation

The Keyser Formation was deposited during the Upper Silurian-Lower Devonian and is characterized by thickly bedded limestone. This unit forms moderate ridges of moderately low relief and is 30 meters thick.

Old Port Formation

The Old Port Formation was deposited during the Lower Devonian. This unit has thin-thickly bedded grey limestones, medium-thickly bedded grey to black shales, and interbeds of sandstone, limestone, and shale. The Old Port Formation tends to form moderately low ridges with low relief and is 150 meters thick.

Onondaga Formation

Deposited during the Lower-Middle Devonian, this unit is characterized by thickly bedded interbeds of dark grey calcareous and noncalcareous shales with few interbedded medium bedded limestones. This unit tends to form rolling terrain with moderately low relief and is 30 meters thick.

Marcellus Formation

This dark grey to black carbonaceous homogeneous shale was deposited during the Middle Devonian. Ranging from 105-150 meters in thickness, this unit tends to form undulating hills of moderately low relief.

Mahantango Formation

This formation, deposited during the Middle Devonian, is split into the Lower Member and the Tully Member. The Lower Member is a thickly bedded shale and the Tully Member (30-75 meters thick) is a thin-thickly bedded limestone. This formation tends to form rolling hills of moderately low relief and is approximately 350-515 meters thick in total.

Harrell Formation

The youngest formation in the Muncy study area is the Harrell Formation that was deposited during the Upper Devonian. This unit is a dark grey to black homogeneous shale with very thick bedding. This unit forms moderately low terrain of low relief and is 45-50 meters thick.

Surficial Geology
Sedimentology

The study area is located on Pleistocene to Recent deposited sediments that are predominately alluvial terrace sediments and alluvium (**Figure 3)**. The alluvial terrace sediment is a moderately to well-sorted deposit of sand and gravel that sit above the floodplains throughout the valley. The silt and sand grains are predominantly quartz with larger grains consisting of red and grey siltstone and sandstone granules and pebbles. Alluvial terrace deposits are variable in thickness but are commonly found to range from 5 to 30 meters. The alluvium deposits are composed of moderately to well-sorted sand and gravel. The silt and sand grains are predominantly quartz with larger grains consisting of red and grey siltstone and sandstone granules and pebbles. Alluvium deposits are found on the valley floor and are extensive along the Susquehanna and Muncy Creek Valleys. Alluvium deposits are variable in thickness but are commonly 5 to 15 meters with a maximum of approximately 30 meters (Faill, 1979).

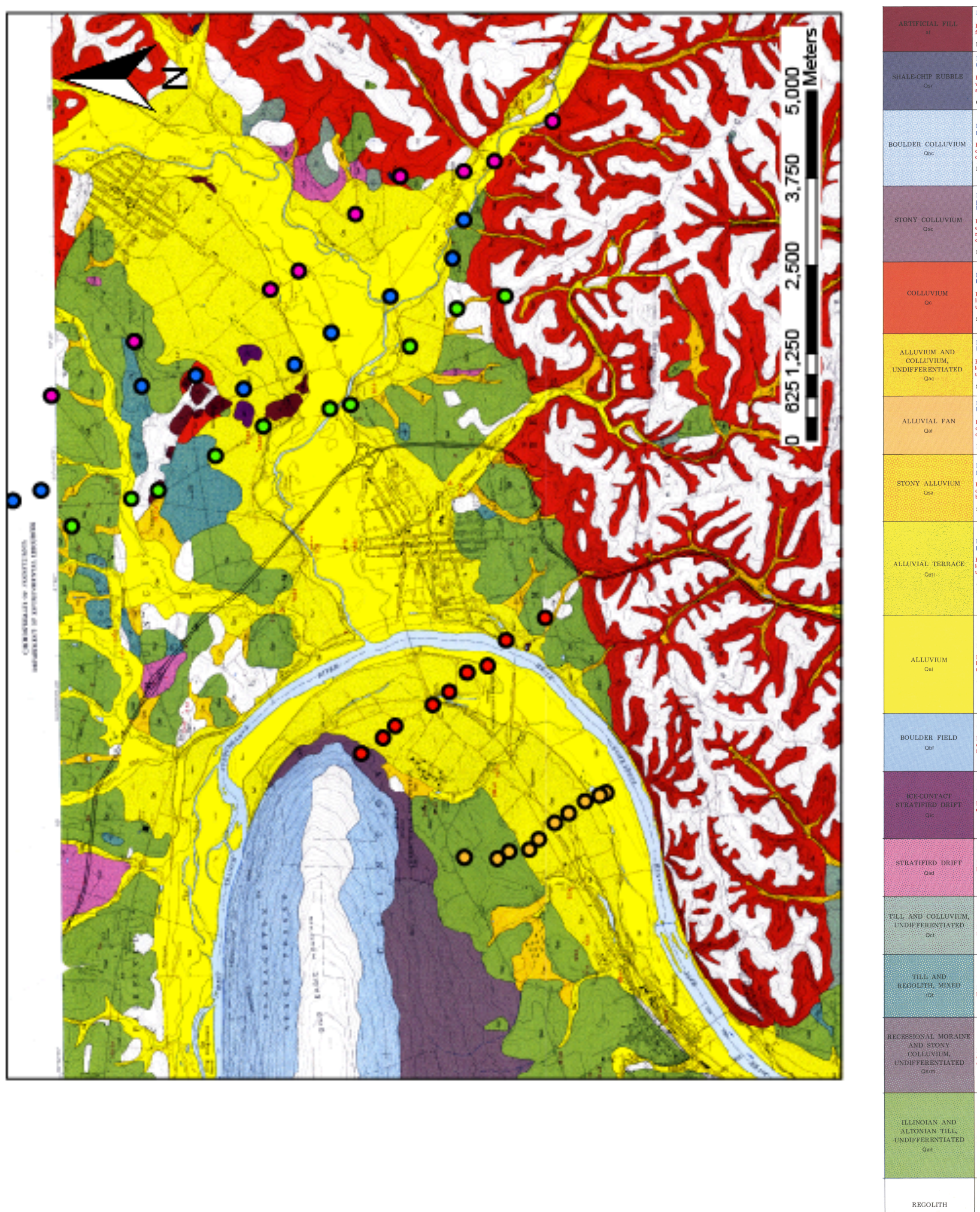

Figure 3: Surficial Geologic Map with unit identification (Faill, 1979).

Depth to Bedrock

Drilling records from water wells in the Williamsport region report the altitude of land surface, depth of the well, and the drill casing depth (Lloyd, O. B., Jr., and Carswell, L. D. et al., 1981), but there is no published synthesis providing a map of depth to bedrock. From these data, the report produced an alluvium saturation thickness map that shows a thickening of the saturated alluvium towards the center of the valley with a thinning of the saturated alluvium towards both bedrock ridges (Lloyd, O. B., Jr., and Carswell, L. D. et al., 1981) (**Figure 4**). This map also shows that the thickest saturated material is located near the nose of Bald Eagle Mountain (labeled on the map), as well as near the center of the valley near Muncy Creek. Based on **Figure 4** our preliminary understanding of the subsurface topography in the region was that of a trapezoidal valley-fill geometry that mimicked the geometry of the saturated alluvium where depth to bedrock is thickest in the middle of the valley (corresponding with the thickest alluvium) and thinnest toward both of the bedrock ridges (**Figure 5**).

In order to develop the understanding of the subsurface topography, water well drilling records were used that report depth to bedrock provided by The Pennsylvania Department of Conservation and Natural Resources' Pennsylvania Ground Water Information System (PaGWIS).

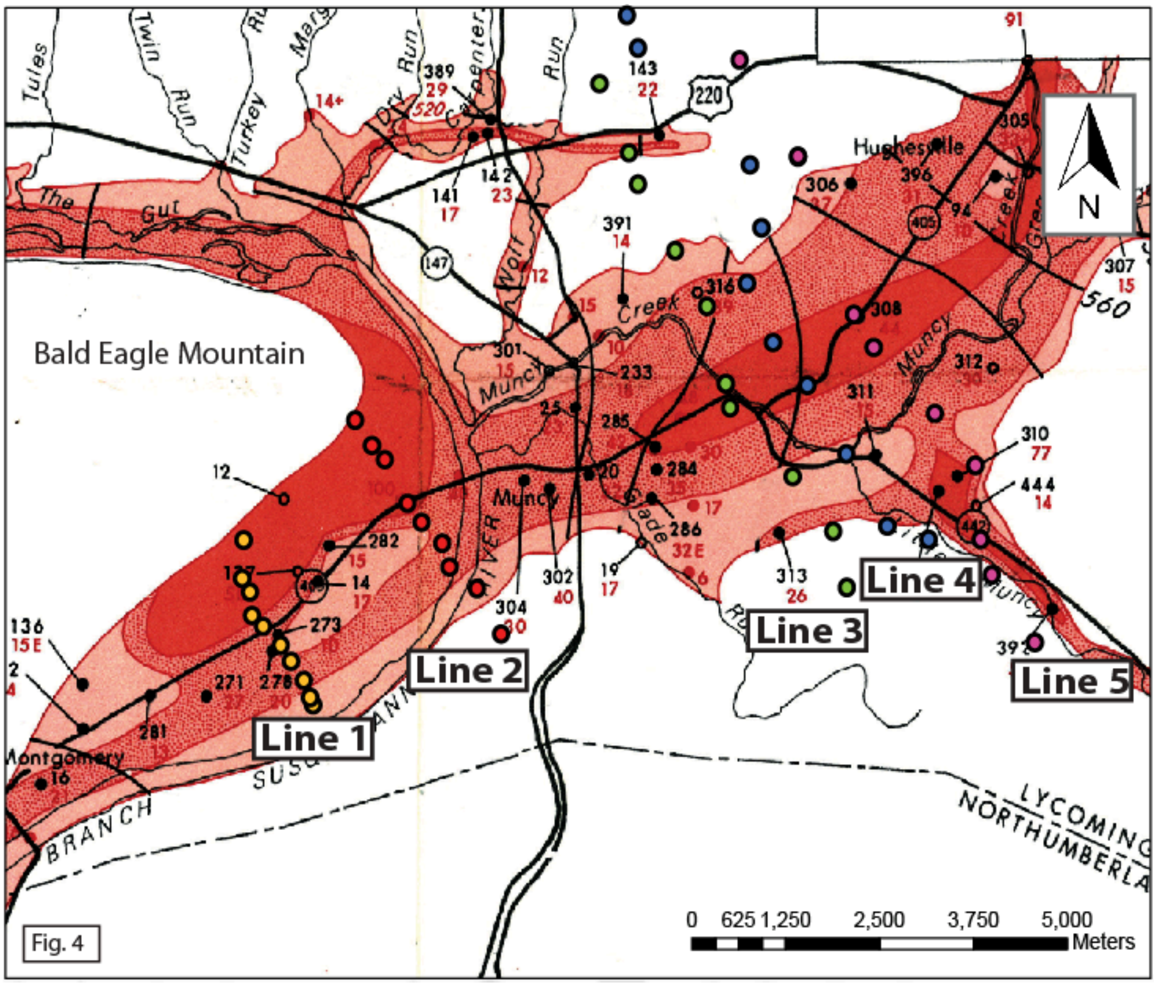

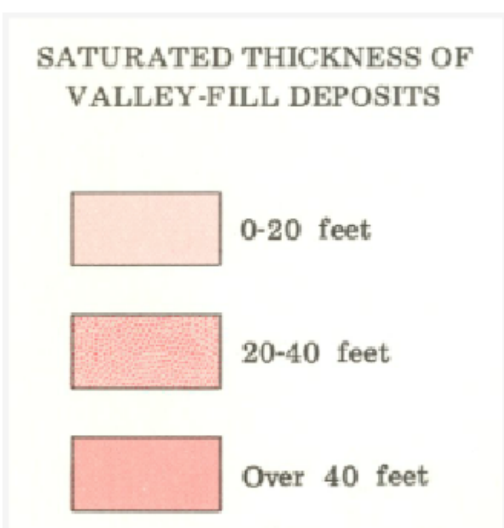

Figure 4: Saturated alluvium thickness map for the Muncy area with the gravity station locations plotted on top (Lloyd, O. B., Jr., and L. D. Carswell, 1981)

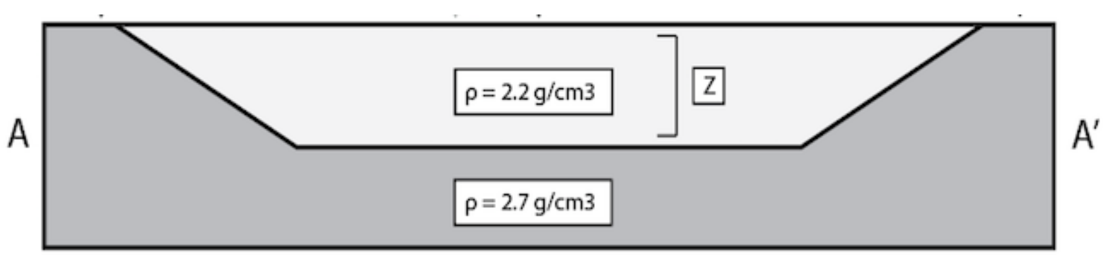

Figure 5: Preliminary understanding of the alluvium-bedrock interface.

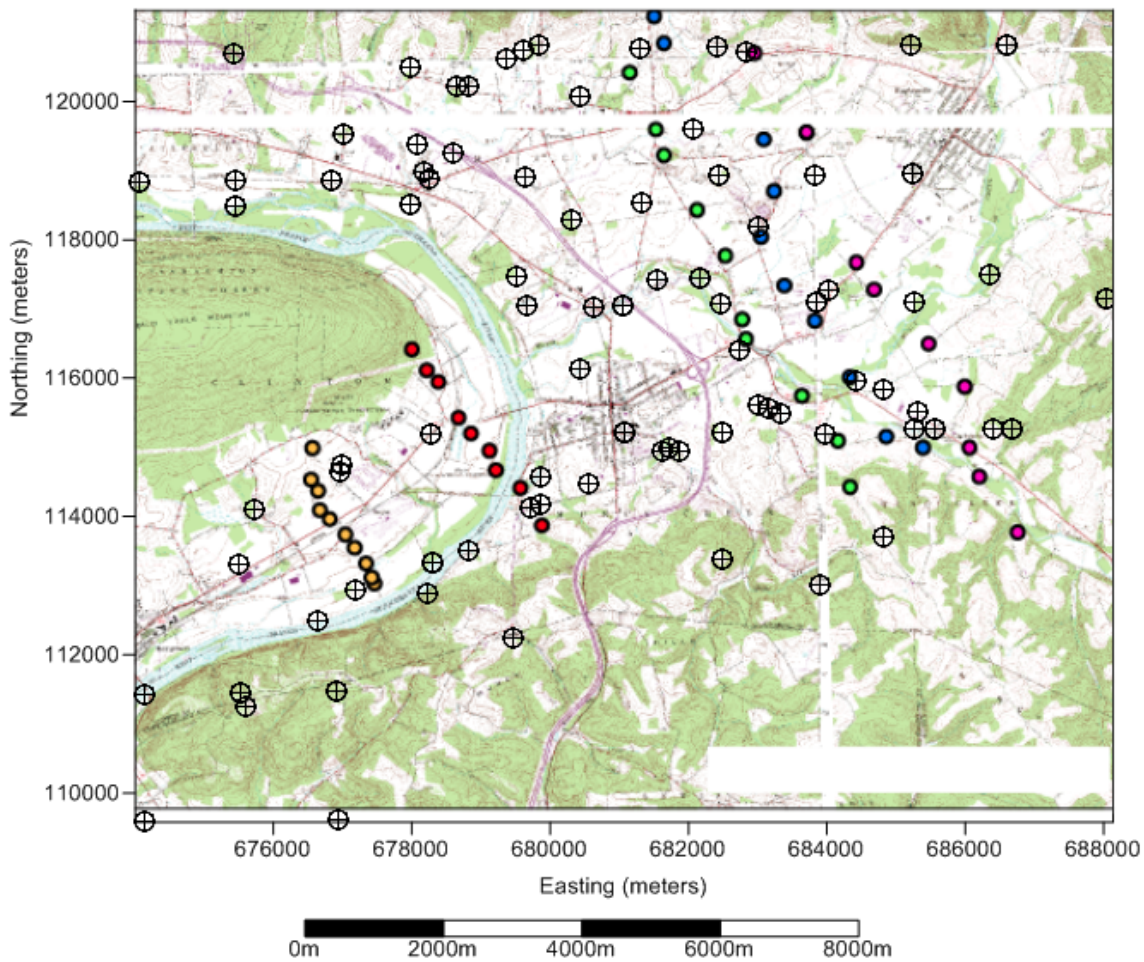

Figure 6: Locations of the well data accessed in the study area. The black circles with crosses represent the well locations and the colored circles represent the gravity stations.

The Gravity Method

Gravity variations arise due to differences in the density of subsurface material from one location to another. For example, a location sitting directly on bedrock will produce a smaller gravity anomaly while a location with a thicker unconsolidated zone will produce a larger gravity anomaly **(Figure 7)**. The difference is directly attributed to the density and thickness of the subsurface material. The typical density of crustal material in earth is 2.7 g/cm^3. The density of the saturated unconsolidated material may be estimated using Equation 1 (Sharma et al., 2006).

$$\rho_{sm} = \rho_{min}\left(1 - \frac{p_{\%}}{100}\right) + \frac{\rho_{\%}}{100} \qquad (1)$$

Where ρ_{sm} is the density of the saturated material, ρ_{min} is the density of the mineral that the material is made of, and $\rho_{\%}$ is the percentage of porosity. Using ρ_{min} as the average crustal density (assumed average bedrock density) and a $\rho_{\%}$ of 30% as the average porosity of alluvial sand and gravel (Fetter et al., 2000), the ρ_{sm} is estimated to be 2.2 g/cm^3.

The expected gravity variations across the Muncy area may be calculated using simple subsurface geometries based on changes of thickness of the unconsolidated section and the estimated densities. Telford et al. (1990) present **Equation 2** to calculate the gravity effect of a 2-D truncated semi-infinite slab model (truncated in profile, infinite in perpendicular horizontal direction).

$$\Delta g = 2G\Delta\rho t\left(\frac{\pi}{2} + \tan^{-1}\frac{\square}{h}\right) \qquad (2)$$

Where Δg is gravity anomaly due to the presence of the slab in mGal, G is the universal gravitation constant (6.67×10^{-11} $m^3kg^{-1}s^{-2}$), $\Delta\rho$ is change in density of the slab material compared to bedrock (g/cm^3), t is the thickness of the slab (m), x is the horizontal position of the measurement location relative to the location of the edge of the slab (m), and h is the depth to the slab (m). A subsurface model where the thickness of the unconsolidated material is 0 m (depth to bedrock = 0 and thus $\Delta\rho = 0$), this would have a gravity anomaly of 0 mGal. Whereas, in a location where the thickness of the unconsolidated material is 5 m (depth to bedrock = 5 m), x is 100 m, h is 1 m, and $\Delta\rho = \rho_{sm} - \rho_{min} = -0.5$ g/cm^3, the gravity anomaly will be -0.1 mGal. This suggests that alluvium with thickness greater than 5 m will produce a gravity variation greater than 0.1 mGal in the Muncy area.

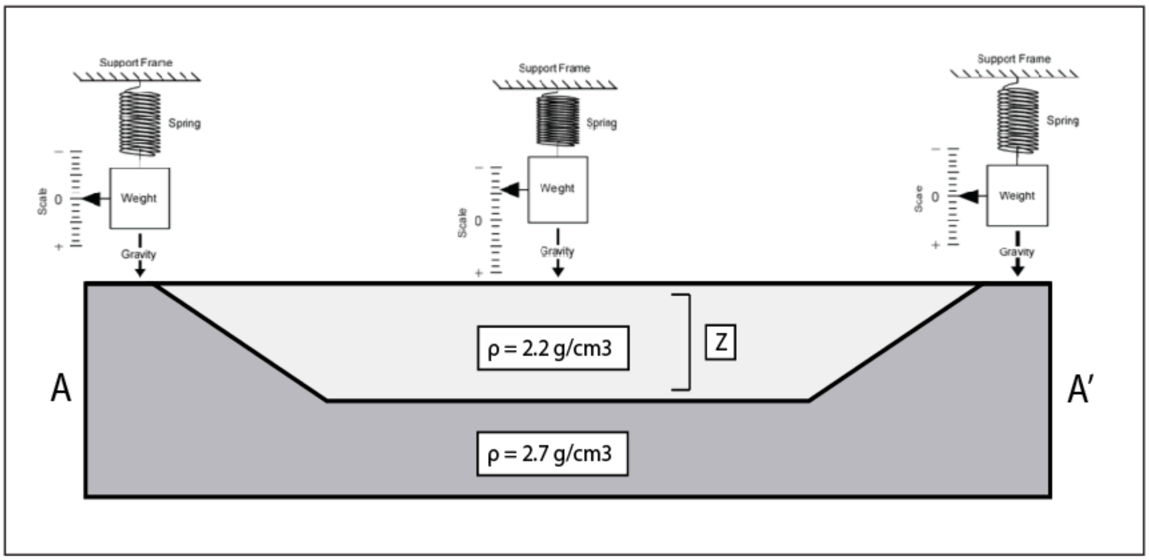

Figure 7: The gravity method. The dark grey represents bedrock while the light grey represents the alluvium.

Methods

Gravity Measurement Procedure

For this study, a LaCoste and Romberg Gravitron gravimeter was used to measure gravity at each of the stations marked in (**Figures 2, 3 and 4**). This instrument has a precision of 0.003 mGal in field conditions (LaCoste, 2002), which suggest that the gravity variation expected from a 5 m thick unconsolidated zone with a 0.5 g/cm^3 density difference will be well resolved**.**

The procedure established for setting up a gravity measurement site for this study was to first pick a location without sharp local topography, away from sources of large high seismic noise as well as away from areas of unstable ground. Once this station had been selected, a sun block (shown in **Figure 8**) was set up to protect the LCD screen on the gravimeter from becoming overheated. This block also acted as a wind-break and reduced the vibrational noise associated with wind. The gravimeter was then placed underneath the sunblock and attached to an external power source located several feet away. By firmly pushing down on the gravimeter after placement, the ground directly in contact with the legs of the gravimeter is packed down, reducing any errors associated with leveling adjustments on soft ground.

The procedure for measuring gravity on the transect lines was to establish two gravity base stations for each unique line. For each gravity base station on a transect line, a 15-minute measurement was taken about every 1-2 hours throughout the day (Sharma et al., 1986) **(Figure 9)**. At all other measurement locations, gravity was measured for at least five minutes. At all stations, the procedure followed was to power on the gravimeter, record measurements for 2 minutes as a calibration, power off then power back on the gravimeter, and then take either the station or base station measurement. The gravimeter recorded a measurement every 20 seconds, resulting in 15 measurements per station and 45 measurements at each base station. Additionally, at each station, to improve data quality, the operator walked away from the gravimeter after the start of data measurement, and only returned at the conclusion. The display on the gravimeter was set to display 5 minutes of data in order to preliminarily analyze the quality of the data and assess if a re-measurement was required. During post-processing, the first and last measurements were discarded (i.e. the first and last 20 seconds at each station) to limit any error due to operator movement. The gravity observations were calculated as the median of the 20 seconds gravity measurements at each station. Longer measurement times, or multiple measurements were utilized at some sites, if it was determined that the drifting of the spring was having an effect on the data. If other errors, such as passing trains, were found to have an effect on the data, then the affected data was not used to calculate the average and median gravity measurements for each gravity station.

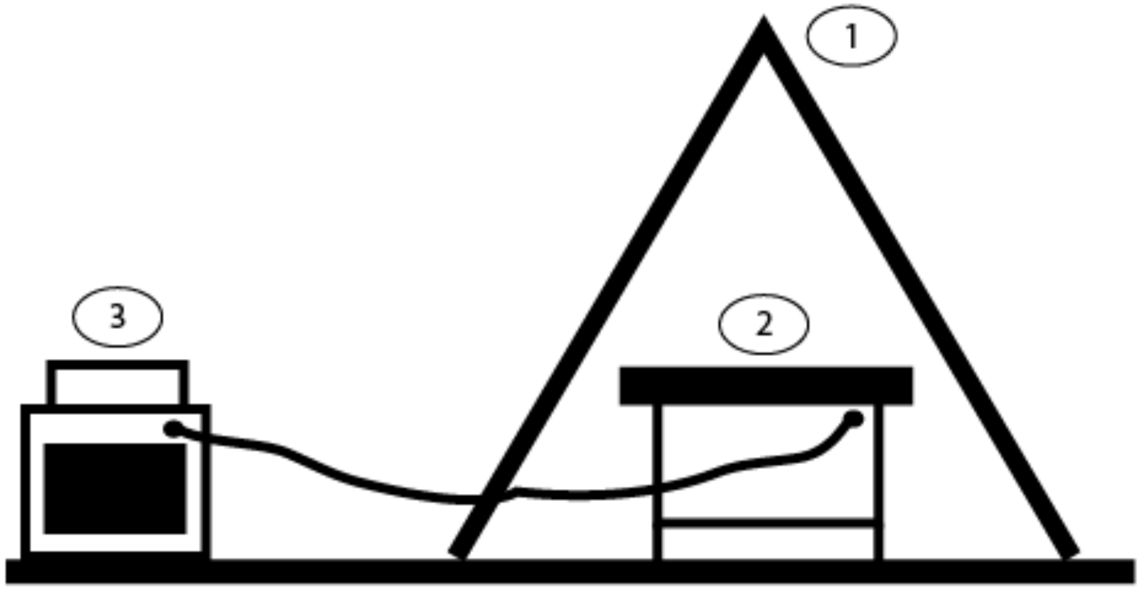

Figure 8: A schematic of the gravimeter positioning at all field sites. (1) wind/sun cover, (2) gravimeter, and (3) external battery for the gravimeter.

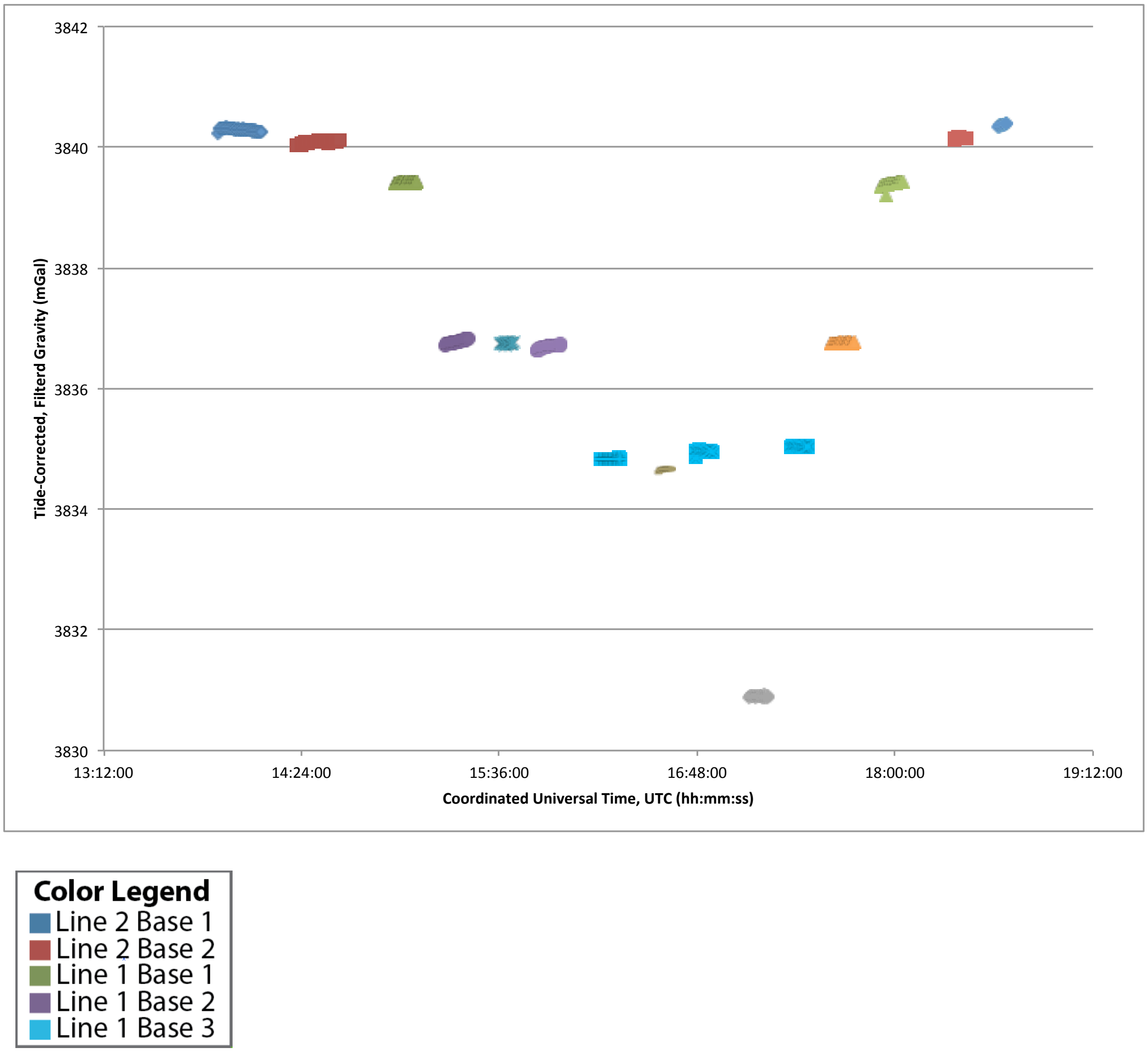

Figure 9: This figure illustrates the base station looping technique that was employed during data collection. By revisiting multiple base stations (like colors on the graph) meaningful data was collected and could be used fully characterize the drift associated with the gravimeter.

Station Positioning

In the field, a Trimble R8 Model 3 Global Positioning System (GPS) with real-time kinematic (RTK) corrections was used to collect elevation and Latitude/Longitude (Lat/Long) coordinates of each gravity station depicted in (**Figures 2, 3 and 4**). The procedure for each field day was to set up a GPS base station, which collected data throughout the day. Once this data had been collected, it was uploaded to the National Oceanic and Atmospheric Administration (NOAA) server for post-processing via the Online Positioning User Service (OPUS). OPUS provides access to the high-accuracy National Spatial Reference System (NSRS) coordinates from the National Geodetic Survey (NGS), a division of NOAA. Once this post-processed information returned from OPUS, the data obtained a horizontal accuracy of ≤8mm and a vertical precision of ≤15mm (Trimble, 2013). In order to assess this precision, specific locations were measured multiple times with the GPS, and through differences in the recorded data the precision and accuracy of the GPS positions were established. Our GPS data was also compared to the 1 meter Digital Elevation Model (DEM) for the region **(Figure 10A-E)** to assess and demonstrate the quality of the elevation data gathered in the field.

Figure 10A

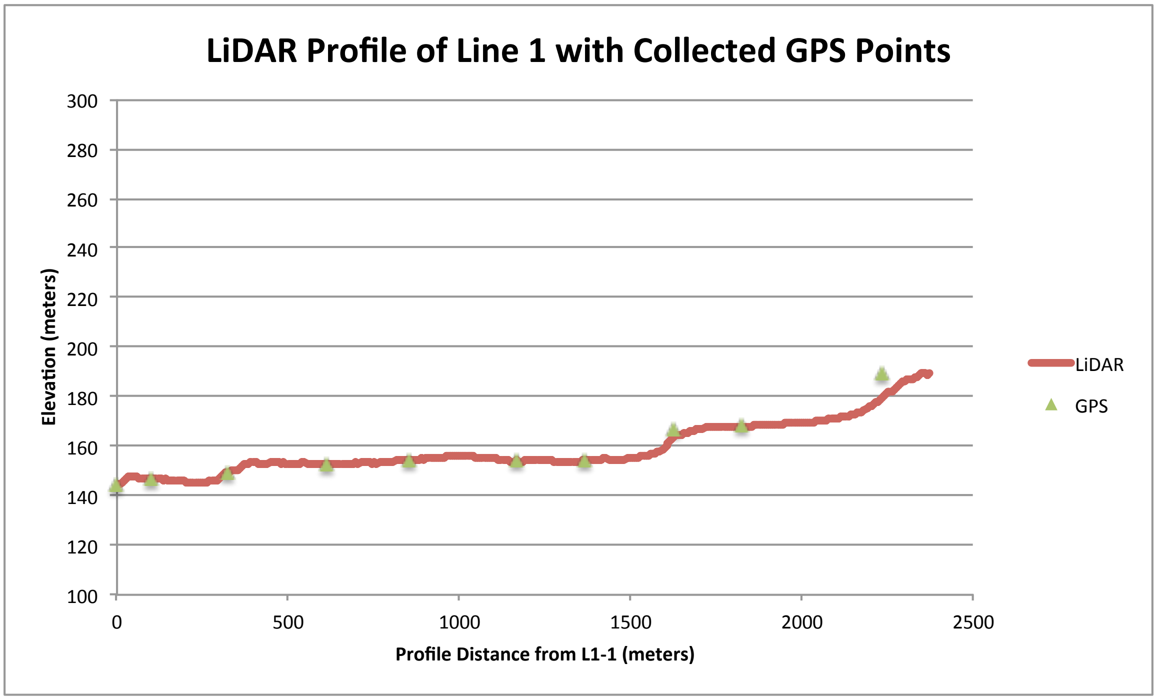

Figure 10B

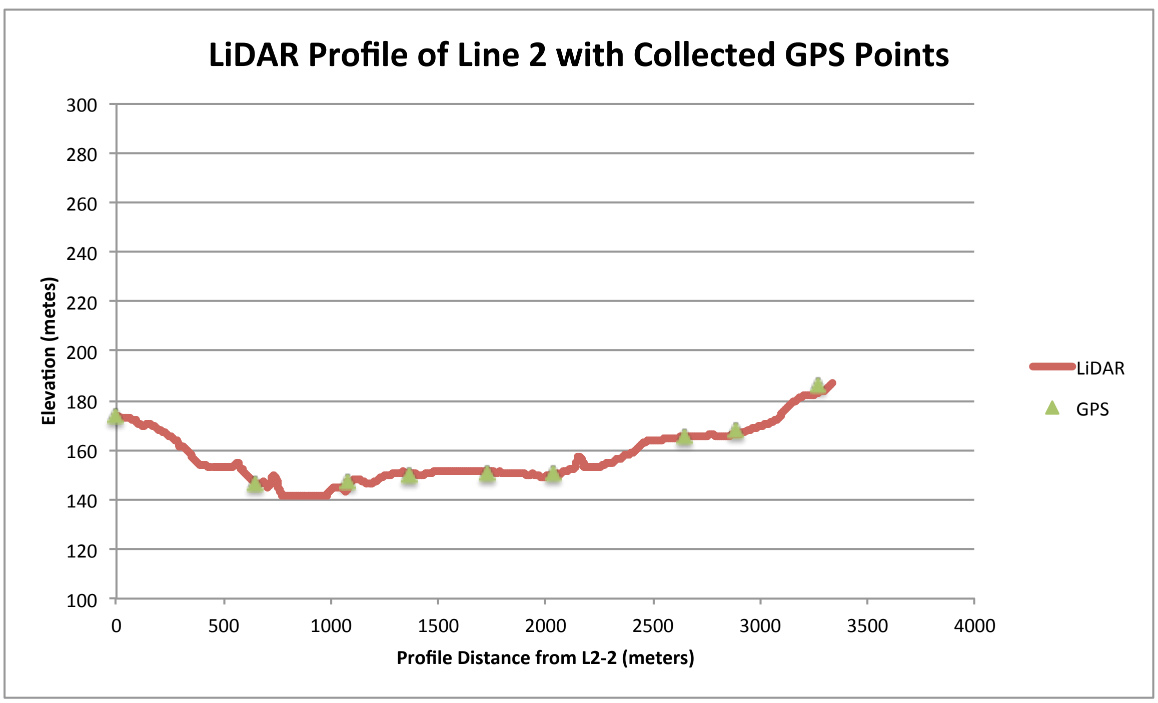

Figure 10C

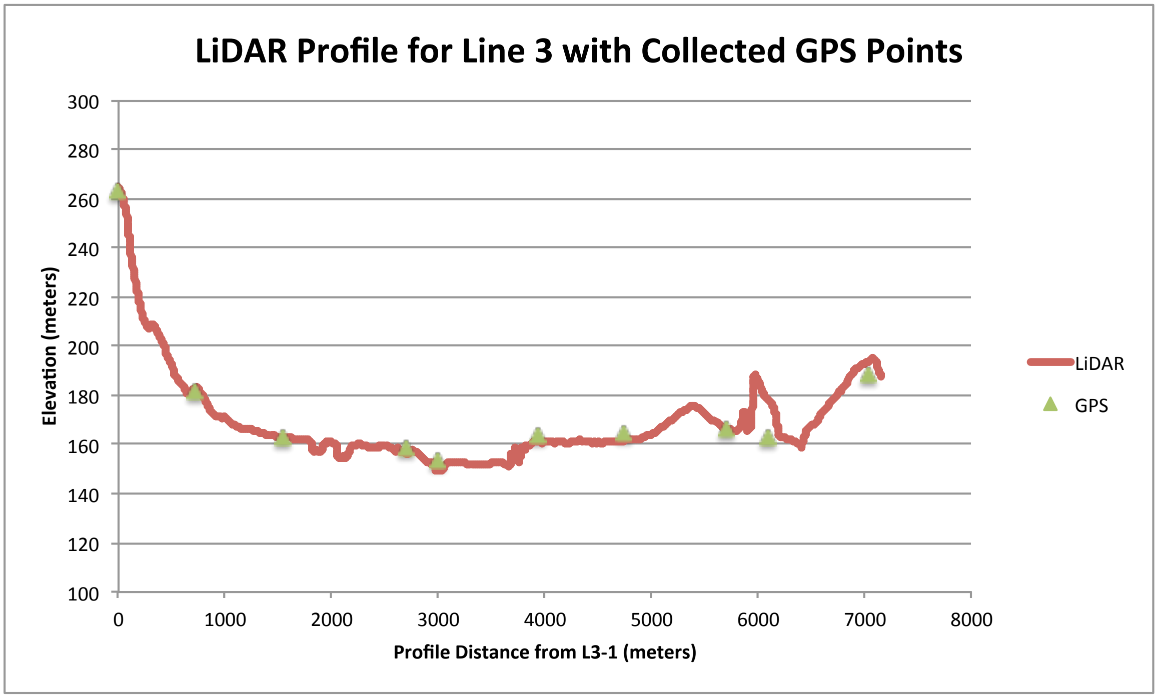

Figure 10D

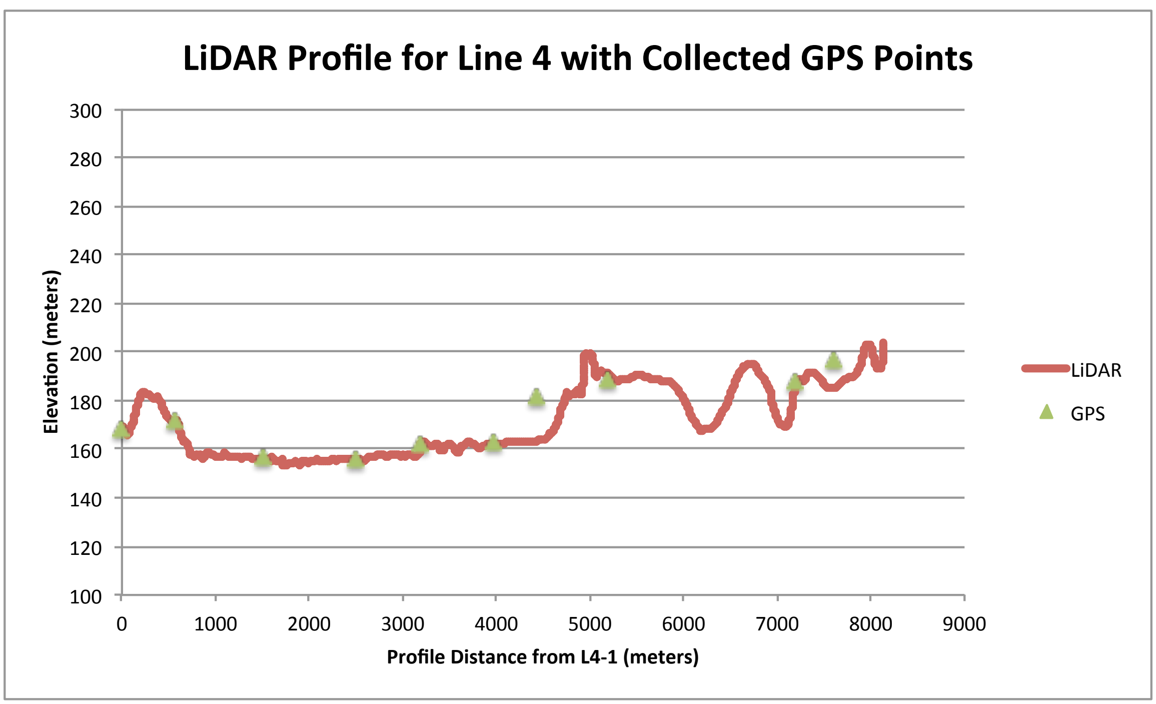

Figure 10E

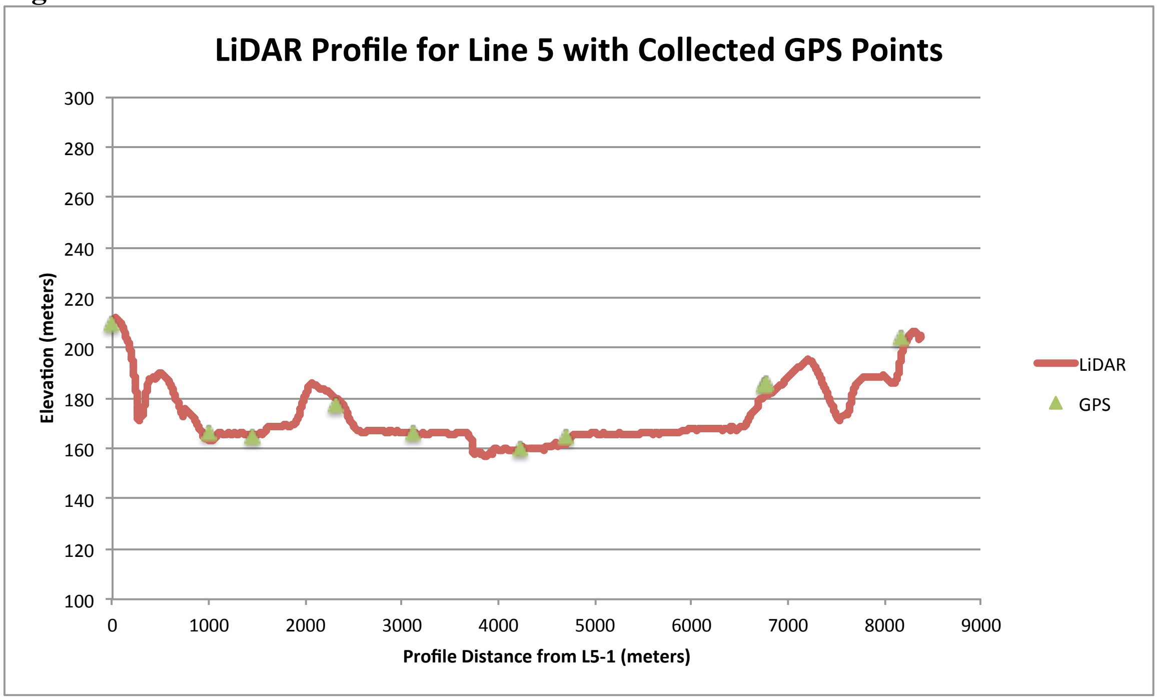

Figure 10A-E: The Light Detection and Ranging (LiDAR) profile of each line along with the GPS point collected for each gravity station.

Post-processing gravity data

To process the data from the base stations (15 minutes) into station observations, the first and last 20 seconds of each measurement were discarded to exclude error due to operator movement. The data was then averaged, the standard deviation and 95% confidence interval were calculated, and a drift rate between base stations was established **(Figure 11)**. The 95% confidence interval was used to describe the noise in the data set (Byler et al., 2012).

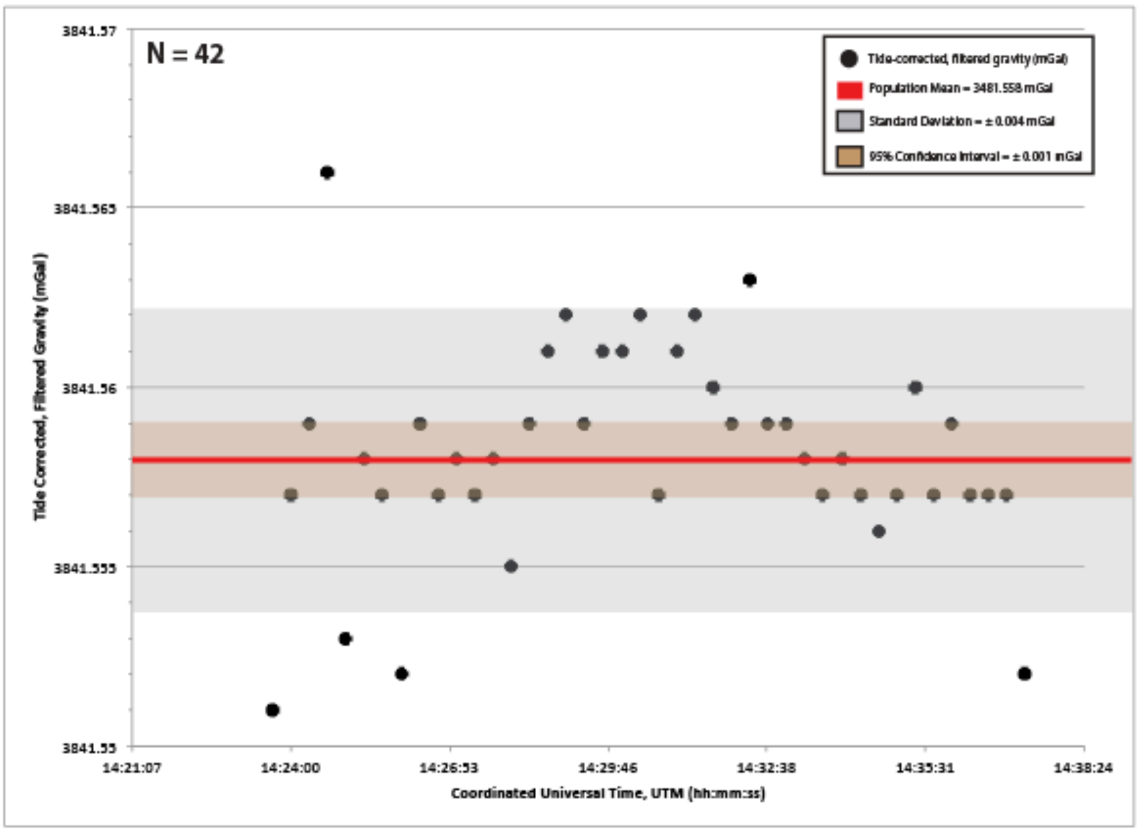

Figure 11: Tide-corrected, filtered gravity base station data collected on July 30th, 2013 at gravity station 5 of line 4 (L4-5). 85.7% of these data are within ±0.004 mGal of the population mean. 95% confidence that the true mean gravity at this location is within ±0.001 mGal of the population mean based on these data.

Before the measured gravity observations can be used to estimate depth to bedrock, six different corrections must be applied.

1. The first correction that was applied to the data was the Earth tidal correction. This correction accounts for variations in the value of gravity due to the position of the moon, the sun and other celestial bodies. Over an interval of 1 to 2 hours, the tidal effect can be well approximated as a strait line and removed. Through a standard proprietary computer program, this correction is calculated internally by the gravimeter and applied to each measurement (L&R, 2002).

2. The second correction that was applied is for correcting the drift of the spring within the instrument. To correct for this, I employed two different methods, site calibration and station looping. The first technique, site calibration, uses a 2-minute measurement, called a calibration, which occurs before the actual gravity measurements are taken. The calibration technique is used to assess the stability of the sensor to tares (a sudden jump in gravity readings), which are a very common occurrence in L&R gravity meters (Ander et al., 1999). In the second method, station looping, one returns to an established base station every 1 or 2 hours to allow for the assumption of linear drift (Sharma et al., 1986). From the station looping technique, one can establish a drift rate by subtracting the initial and final base station gravity readings and dividing by the elapsed time between the station occupations (**Equation 3**). Once the rate is established, gravity

readings collected in the time period between the base station occupations can be corrected.

$$drift = \frac{g_0 - g_t}{\Delta t} \quad (3)$$

Where g_0 is the initial base station, g_t is the same base stations at Δt (time) after the initial measurement.

3. Due to the ellipsoidal shape of the earth and the centrifugal force from earth's rotation (maximum at equator and zero at the poles), the value of gravity increases with increasing latitude. The latitude correction was based off of the increasing change in latitude between the most southern station and the progressively more northern stations. To correct for this phenomena, the latitude correction will be added to the data except for the most southern station. This correction is made by applying **Equation 4**, which assumes the radius of the earth has minimal change and that ϕ is the latitude of an arbitrary station (Sharma et al., 1986).

$$C_\phi = 0.812\ sin2\phi\ mGal/km \quad (4)$$

4. The Free-air correction accounts for the effect of earth's weakening gravitational field with an increase in elevation. The standard compensation adds 0.3086 mGal for every meter of increase in elevation as seen in **Equation 5**, where *h* is the elevation in meters and it is assumed that the change in the radius of the earth is negligible (Sharma et al., 1986).

$$C_F = 0.3086\Delta h\ mgal \quad (5)$$

5. The next correction, the Bouguer correction, accounts for the increase in mass of the underlying material that is associated with an increase in elevation. As the elevation increases, the correction is subtracted from the observation. To account for this mass increase, **Equation 6** was applied to the collected data, where *h* is the elevation in meters and ρ is the surface density g/cm^3. (Sharma et al., 1986).

$$C_B = 2\pi\rho h = 0.0419 h\rho \; mGal \tag{6}$$

6. The last elevation correction, the Terrain correction, accounts for the gravitational anomalies associated with the surrounding topographic features. The Terrain correction has two component of error (1) based on the amount of material present above and absent below an assumed flat surface through the station. This estimate must be made quite accurately near the station, but for areas farther away, approximation is possible. (2) The Terrain correction employs a density correction. By using Geosoft's Oasis software package along with Pennsylvania LiDAR 1 meter Digital Elevation Model (DEM) data, the terrain correction was calculated and applied to the collected data.

After the application of these six corrections, the corrected gravity data can now be referred to as the Bouguer Anomaly (Δg) and used to evaluate the changes in the thickness of the surface density material.

Results

Bouguer Anomaly Data

Line 1

Located in the southwestern corner of the study area, this transect has 10 gravity stations spread over a distance of approximately 2,000 meters **(Figure 12)**. This line begins on the northeast edge of the WBSR and continues northwest to southeastern edge of the Bald Eagle Mountain. The Bouguer Anomaly from Line 1 has a range of approximately 1.050 mGal with a minimum value of 3866.898 ± 0.003 mGal, a maximum value of 3867.948 ± 0.003 mGal and a 95% confidence interval that ranges from 0.002 to 0.012 mGal with a median of 0.004 mGal. This transect has three gravity stations (1 through 3) in the Lower Member of the Mahantango Formation, one gravity station (4) in the Marcellus Formation, one gravity station (5) in the Old Port Formation, one gravity station (6) in the Keyser Formation, one gravity station (7) in the Tonoloway Formation, two gravity stations (8 through 9) in the Wills Creek Formation, and one station (10) in the Mifflintown Formation **(Figure 2)**. Overall, the data show a decrease in gravity from Station 1 to Station 6 corresponding to a thickening of alluvium and then an increase in gravity from Station 6 to Station 10 corresponding to a thinning in alluviu

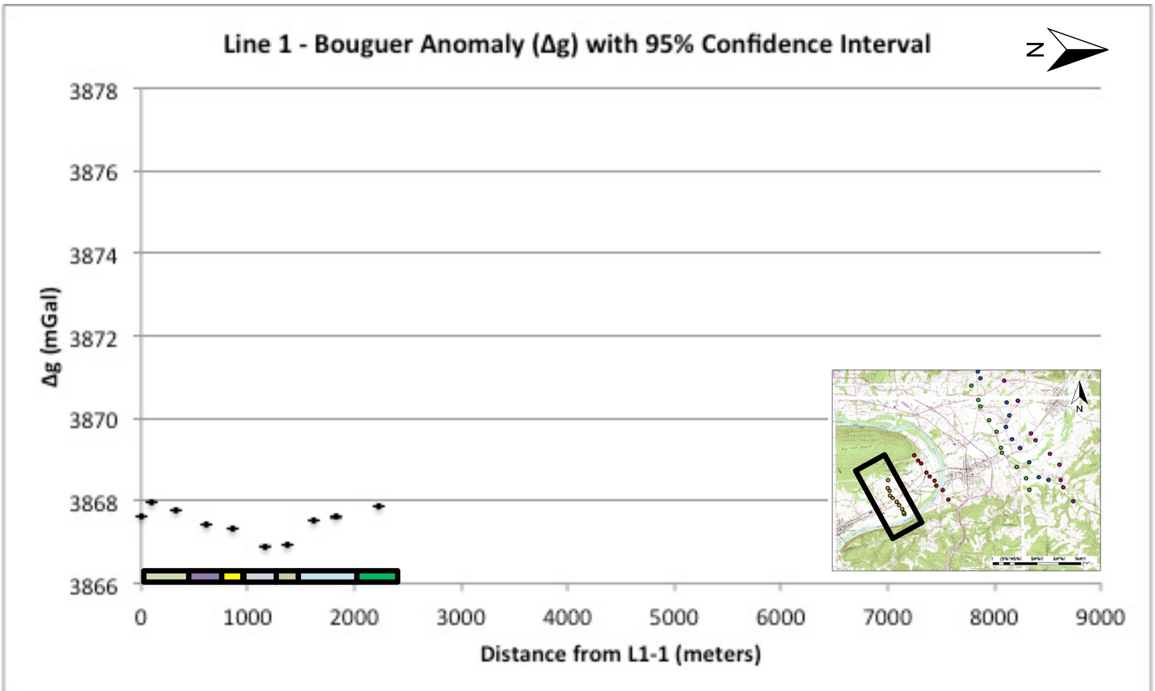

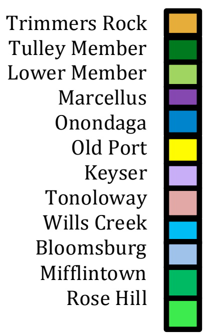

Figure 12: The calculated Bouguer Anomaly for Line 1 with the 95% confidence interval for each gravity station, reference map, and bedrock units associated with the location of each gravity station.

Line 2

Line 2 is northeast of Line 1. This line has 9 gravity stations spread over a distance of approximately 3,300 meters **(Figure 13)**. The first two stations of Line 2 are to the southeast of the WBSR with the remaining 7 stations to the northwest of the WBSR, ending at the eastern edge of Bald Eagle Mountain. The Bouguer Anomaly from Line 2 has a range of 3.255 mGal with a minimum value of 3866.545 ± 0.003, a maximum value of 3869.800 ± 0.003 mGal and a 95% confidence interval that ranges from 0.001 to 0.139 mGal with a median of 0.003 mGal. This transect has one gravity station (1) in the Lower Member of the Mahantango Formation, one gravity station (2) in the Old Port Formation, one gravity station (3) in the Tonoloway Formation, one gravity stations (4) in the Wills Creek Formation, two gravity stations (5 through 6) in the Bloomsburg Formation, and three gravity stations (7 through 9) in the Rose Hill Formation **(Figure 8)**. The data show a decrease in gravity from Station 1 to Station 2 (thickening of alluvium), an increase in gravity from Station 2 to Station 4 (thinning of alluvium), a slight decrease from Station 4 to Station 5 (thickening of alluvium), an increase in gravity from Station 5 to Station 6 (thinning of alluvium), and a decrease in gravity from Station 6 to Station 9 with a sharp decrease from Station 7 to Station 9 (thickening of alluvium).

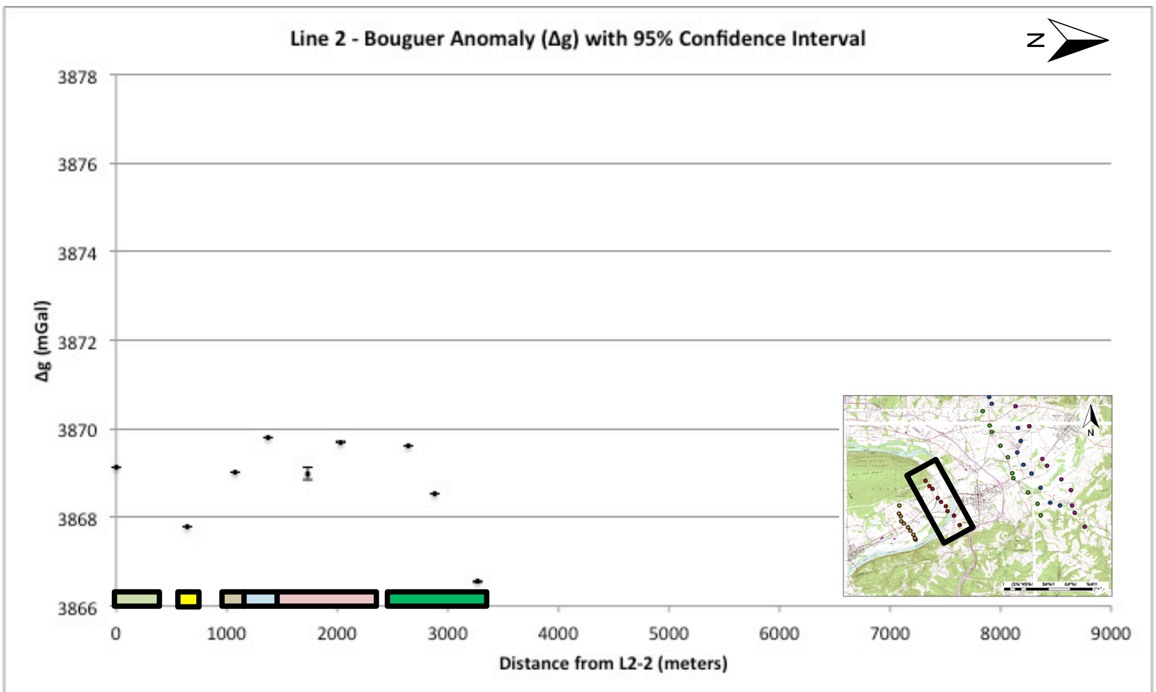

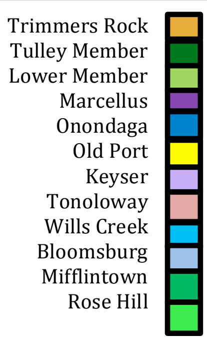

Figure 13: The calculated Bouguer Anomaly for Line 2 with the 95% confidence interval for each gravity station, reference map, and bedrock units associated with the location of each gravity station.

Line 3

This line is located to the northeast of the town of Muncy. This transect has 10 gravity stations spread over approximately 7,000 meters **(Figure 14)**. The first 6 stations are located on the southern limb of the Nittany Anticline, and the remaining 4 stations are located on the northern limb of the Nittany Anitcline. The Bouguer Anomaly from Line 3 has a range of 2.639 mGal with a minimum value of 3871.276 ± 0.003 mGal, a maximum value of 3873.915 ± 0.003 mGal and a 95% confidence interval that ranges from 0.001 to 0.044 mGal with a median of 0.007 mGal. This transect has one gravity station (1) in the Trimmers Rock Formation, two gravity stations (2 and 8) in Lower Member of the Mahantango Formation, one gravity stations (3) in the Marcellus Formation, five gravity stations (4 through 8) in the Tonoloway Formation, and one gravity station (9) in the Old Port Formation **(Figure 8)**. Overall, the data show a decrease in gravity from Station 1 to Station 4 (thickening of alluvium), an increase in gravity from Station 4 to Station 7 (thinning of alluvium), a decrease in gravity from Station 7 to Station 8 (thickening of alluvium), and a slight increase in gravity from Station 8 to Station 10 (thinning of alluvium).

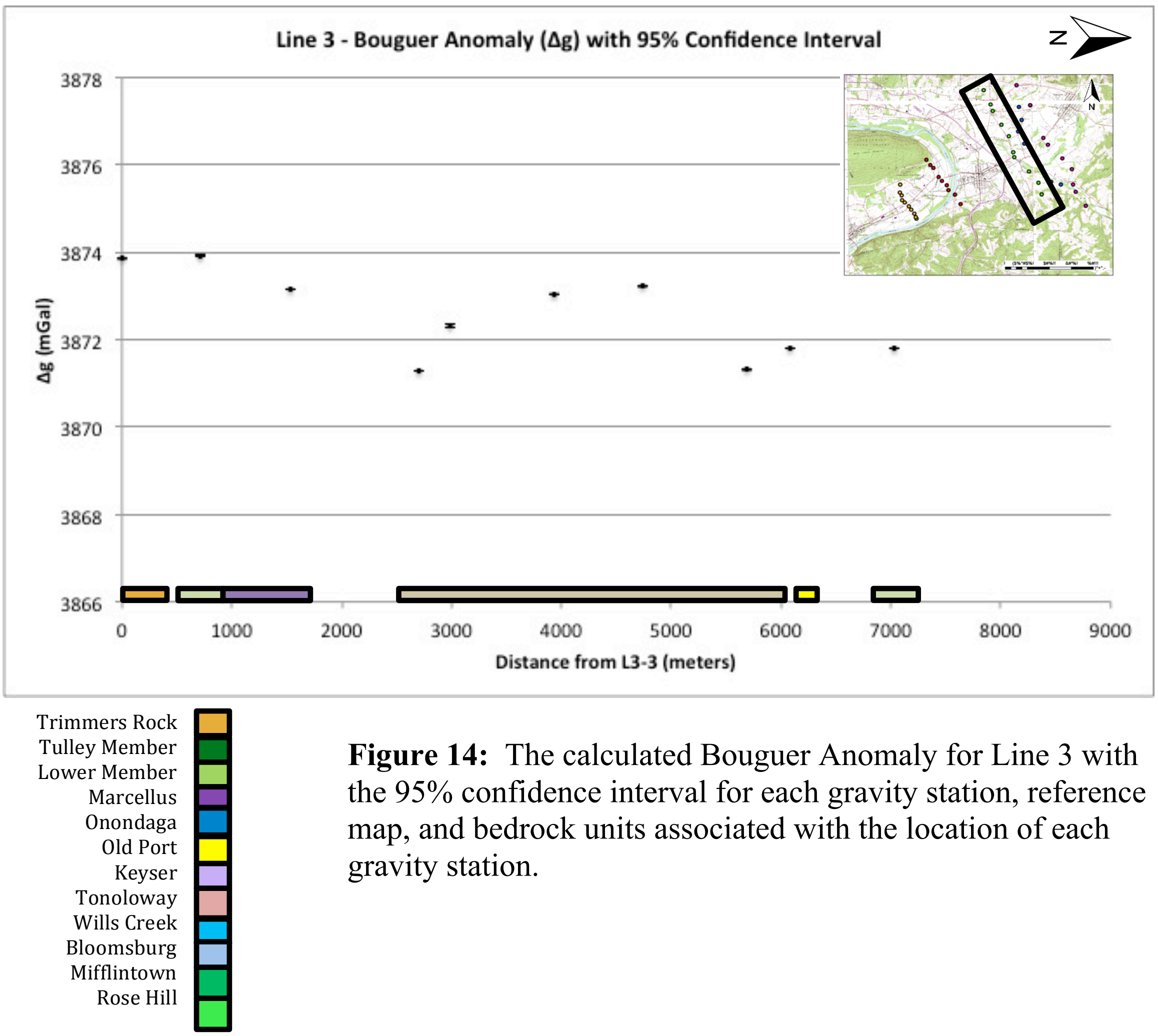

Figure 14: The calculated Bouguer Anomaly for Line 3 with the 95% confidence interval for each gravity station, reference map, and bedrock units associated with the location of each gravity station.

Line 4

Located to the northeast of and roughly parallel to Line 3, Line 4 has 10 gravity stations spread over approximately 7,600 meters **(Figure 15)**. The first five gravity stations are located on the southern limb of the Nittany Anticline with the other 5 gravity stations positioned on the northern limb of the Nittany Anticline. The Bouguer Anomaly from Line 4 has a range of 3.561 mGal with a minimum value of 3870.816 ± 0.003 mGal, a maximum value of 3874.378 ± 0.003 mGal and a 95% confidence interval that ranges from 0.001 to 0.013 mGal with a median of 0.004 mGal. This transect has one gravity station (1) in the Tulley Member of the Mahantango Formation, one gravity station (2) in the Lower Member of the Mahantango Formation, one gravity station (3) in the Marcellus Formation, two stations (4 and 7) in the Old Port Formation, two stations (5 through 6) in the Tonoloway Formation, one gravity station (7) in the Onondaga Formation, and two gravity stations that are located off of the Bed Rock Geology Map **(Figure 8)**. Overall, the Bouguer Anomaly shows a continuous decrease from Station 1 to Station 10 (thickening of alluvium). This decreasing gravity trend is likely not the gravity signature of alluvium thickness, but rather that of deep bedrock structure, which is a plunging anticline for the study area.

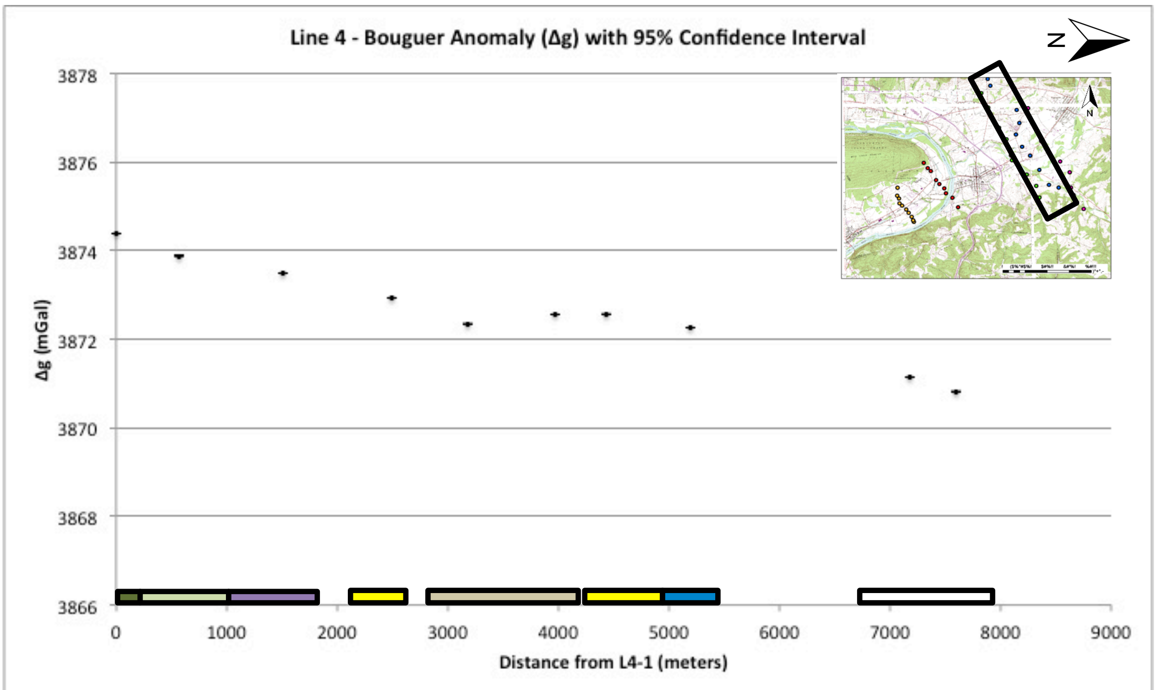

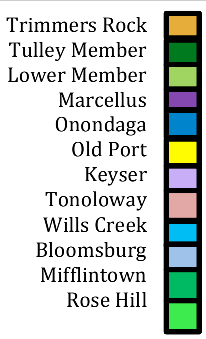

Figure 15: The calculated Bouguer Anomaly for Line 4 with the 95% confidence interval for each gravity station, reference map, and bedrock units associated with the location of each gravity station.

Line 5

Located to the northeast of and roughly parallel to Line 3 and Line 4, Line 5 has 10 gravity stations spread over approximately 8,200 meters **(Figure 16)**. The first seven gravity stations are located on the southern limb of the Nittany Anticline and the remaining three gravity stations are located on the northern limb of the Nittany Anticline. The Bouguer Anomaly from Line 5 has a range of 3.167 mGal with a minimum value of 3873.928 ± 0.003 mGal, a maximum value of 3877.095 ± 0.003 mGal and a 95% confidence interval that ranges from 0.002 to 0.016 mGal with a median of 0.005 mGal. This transect has three gravity stations (1 through 3) in the Trimmers Rock Formation, two gravity stations (4 through 5) in the Lower Member of the Mahantango Formation, three gravity stations (6 and 8 through 9) in the Marcellus Formation, and one gravity station that is located off of the Bedrock Geology Map **(Figure 8).** From Station 1 to Station 10 (thickening of alluvium), there is a continuous decrease in gravity much like Line 4. This decreasing gravity trend is likely not the gravity signature of alluvium thickness, but rather that of deep bedrock structure, which is a plunging anticline for the study area.

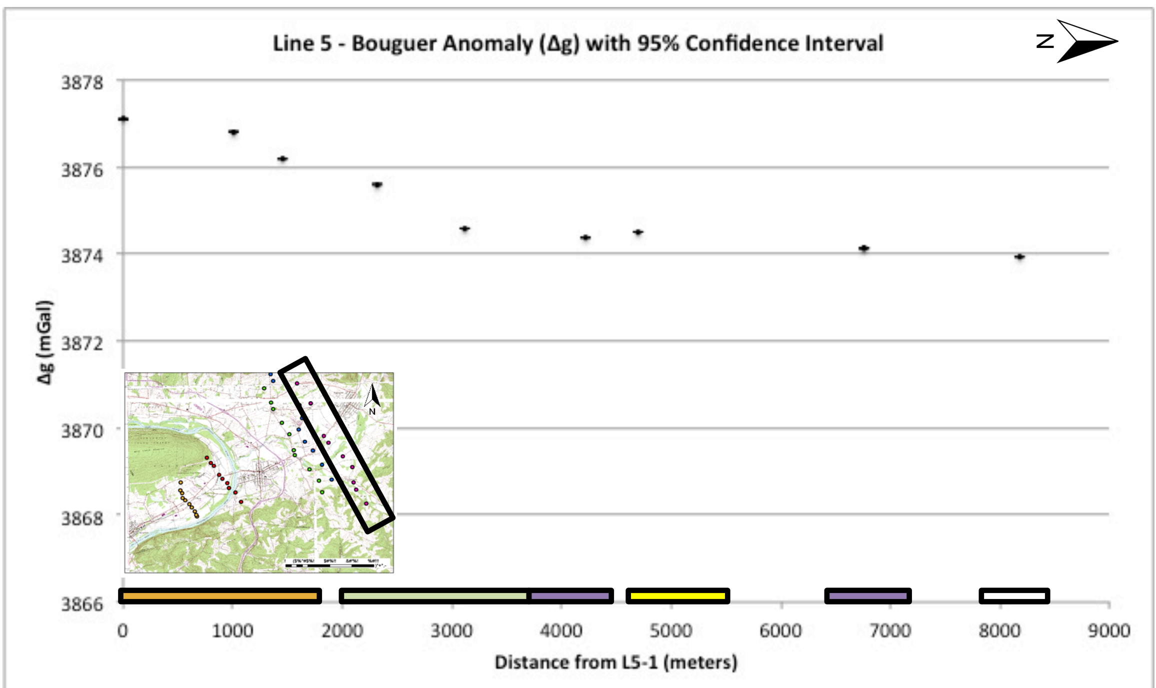

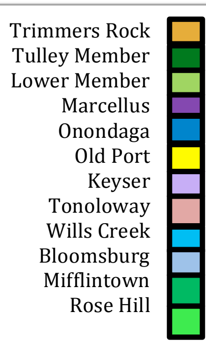

Figure 16: The calculated Bouguer Anomaly for Line 5 with the 95% confidence interval for each gravity station, reference map, and bedrock units associated with the location of each gravity station.

Determination of the Regional

Line 1 supports the hypothesis that alluvium density and thickness variations, decrease in gravity towards the center of the transect and an increase in gravity towards the ends of the transect. Lines 2 and 3 do not obviously reflect the preliminary understanding of the valley-fill geometry like Line 1, but there are both increases and decreases in gravity that could correspond to a more complex model of the bedrock topography like that in the depth to bedrock map determined from well drilling data. Lines 4 and 5 do not reflect the preliminary understanding of the valley-fill, nor does it resemble the more complex depth to bedrock map. Both of the lines show a continuous decrease in gravity from Station 1 to Station 10, leading us to believe that our gravity measurements may be more affected by deeply seated bedrock structures, most likely the Nittany Anitcline, which is masking any valley fill geometries.

To remove the regional effect on our data, a liner regression approach was used, where the data were fitted with a least squares regression line (Telford et al., 1990). Line 4 data was used because of the greatest difference in the first and last gravity values. . The result of our model was a line with a slope of -0.0004. Then the average of the y-intercepts of the least squares regression line for all of the lines was calculated, resulting in a y-intercept of 3872.32. Thus, the equation of the regional was calculated to be:

$$y = -0.0004x + 3872.32 \quad (7)$$

Based on this equation, there is a regional effect of approximately 4 mGal over 7,600 meters, or 0.0004 mGal/meter. The magnitude of our calculated regional is consistent with the Bouguer Anomaly Map of Pennsylvania **(Figure 17)** that reports a regional effect of 5-10 mGal in the approximate study area and immediately surrounding area.

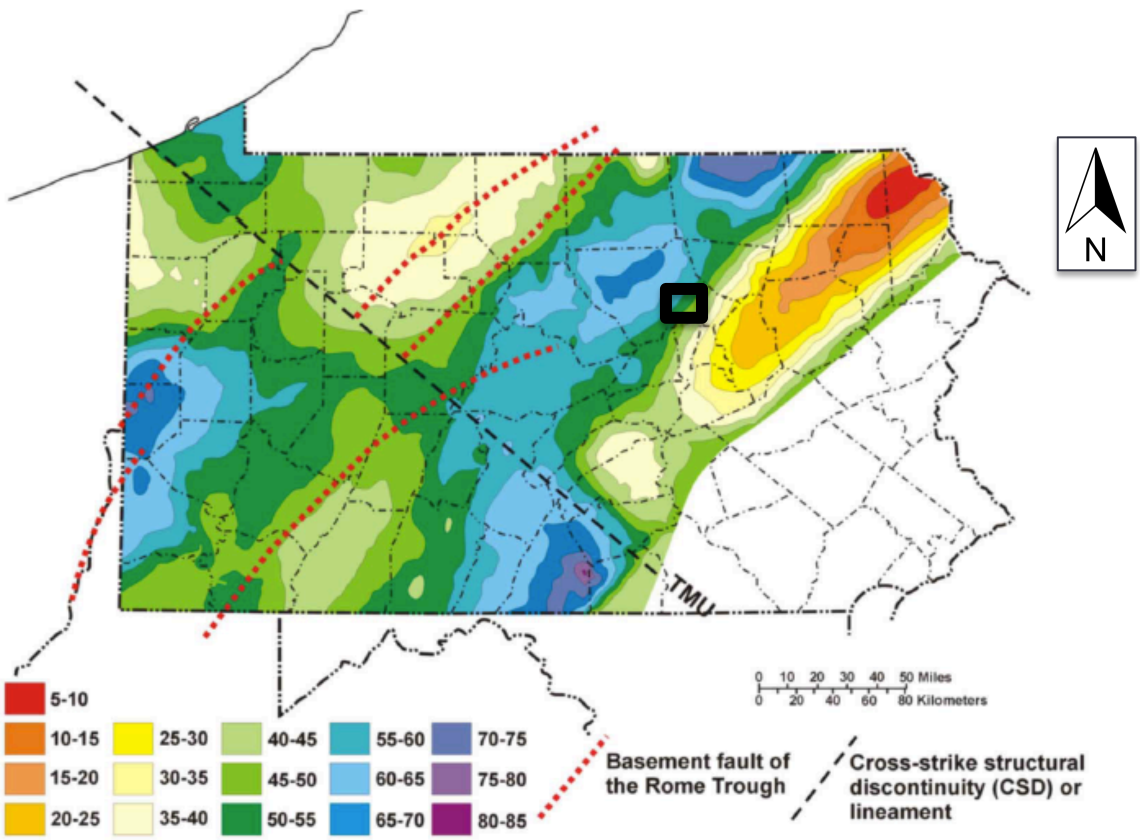

Figure 18: Simple Bouger gravity map of Pennsylvania (adapted from Parrish and Lavin, 1982, supplemented by unpublished data). Contour intervals in milligals (mGal).

Residual Data

The residual was calculated by subtracting the value of y from **Equation 7** from the Bouguer Anomaly value for each gravity station on each transect, resulting in a new value unaffected by the deeply seeded bedrock structures in the area.

Line 1

The calculated residual values for Line 1 **(Figure 18)** have a range of 1.404 mGal with a minimum value of -4.956 mGal and a maximum value of -3.550 mGal. Similar to the Bouguer Anomaly values, the residual gravity values decrease from Station 2 to Station 6 and increase from Stations 6 to Station 10.

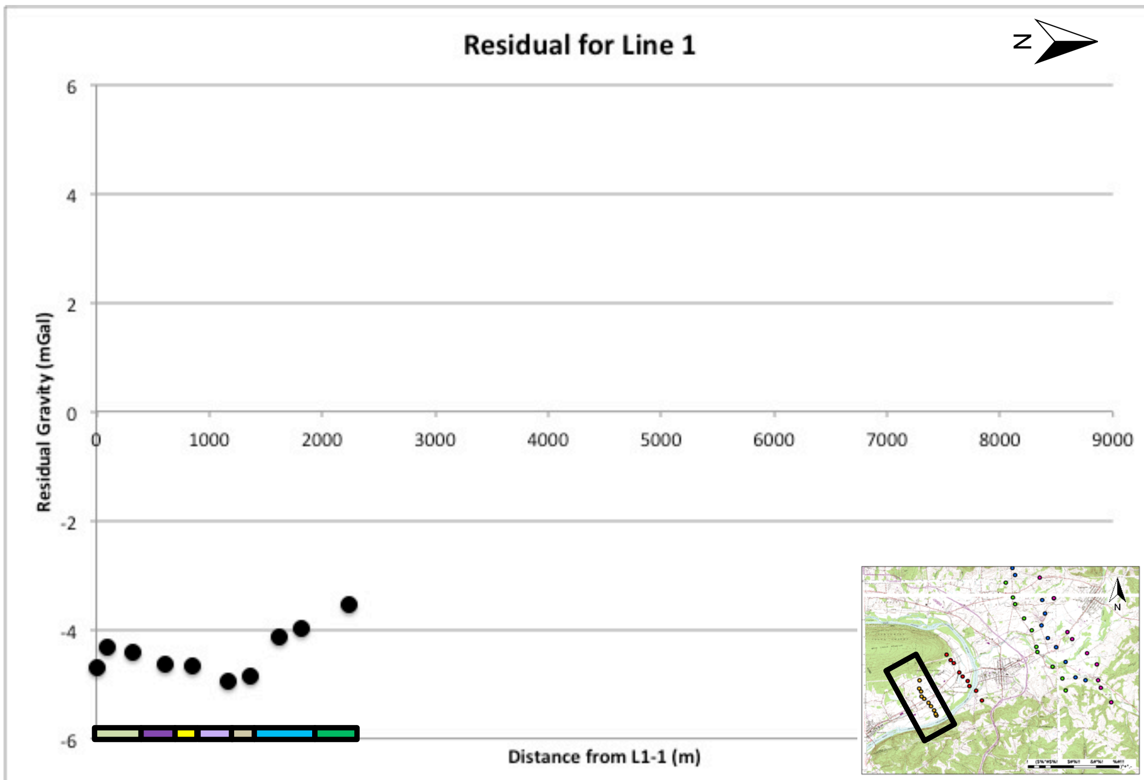

Figure 18: Residual data for Line 1 with reference map and bedrock type associated with the location of the gravity station.

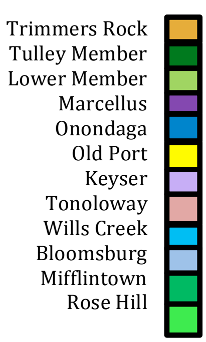

Line 2

The residual values for Line 2 **(Figure 19)** have a range of 2.811 mGal with a minimum value of -4.467 mGal and a maximum value of -1.656 mGal. The residual plot is similar to the Bouguer Anomaly plot, where there is a decrease between Station 1 and Station 2, an increase between Station 2 and Station 4, a slight decrease between Station 4 and Station 5, a slight increase between Station 5 and Station 6 and a decrease between Station 6 and Station 9.

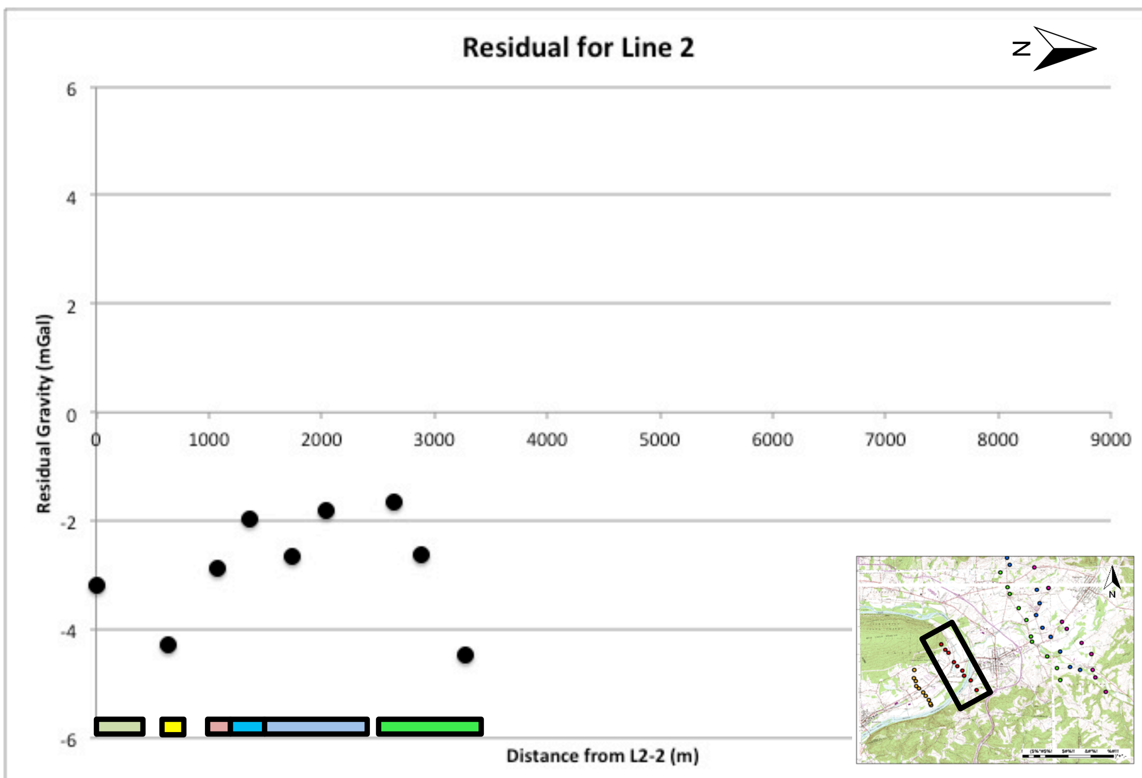

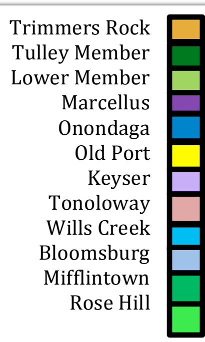

Figure 19: Residual data for Line 2 with reference map and bedrock type associated with the location of each gravity station.

Line 3

The residual values for Line 3 **(Figure 20)** have a range of 2.751 mGal with a minimum value of 0.039 mGal and a maximum value of 2.790 mGal. The residual plot is similar to the Bouguer Anomaly plot with a decrease between Station 2 and Station 4, an increase between Station 4 and Station 7, a decrease between Station 7 and Station 8, and an increase between Station 8 and Station 10.

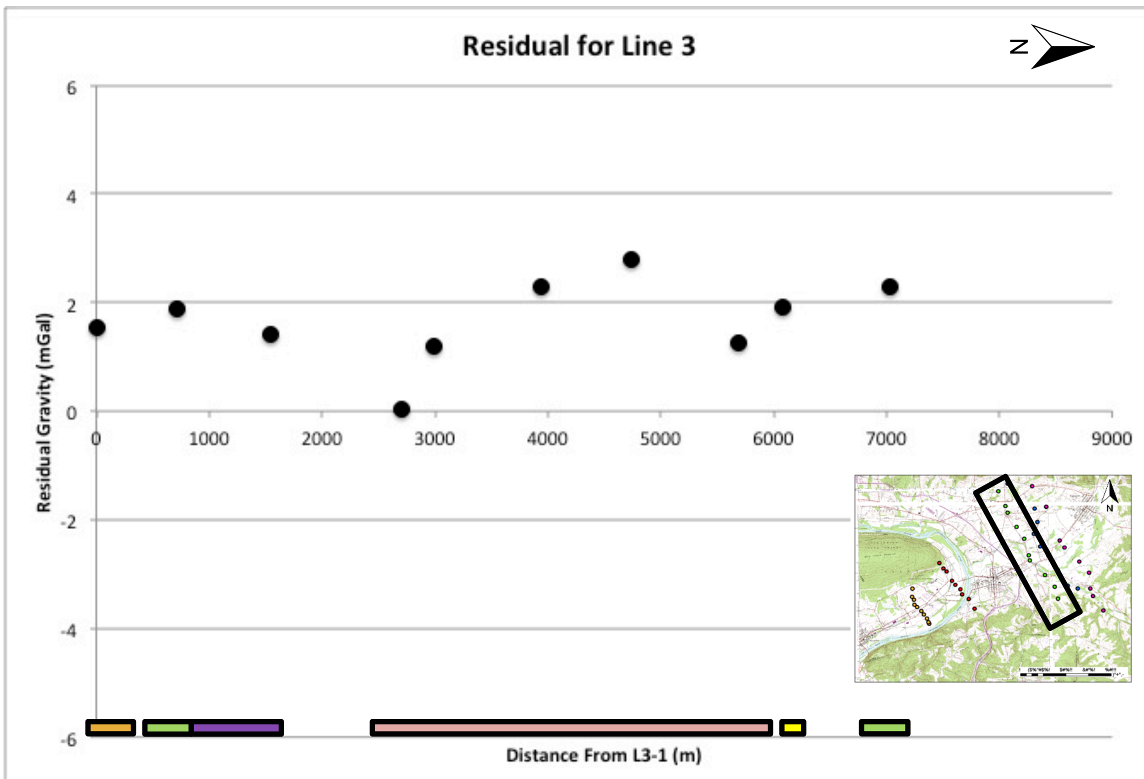

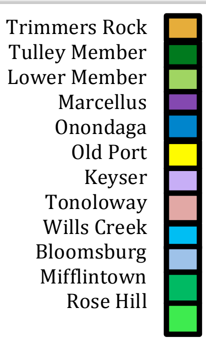

Figure 20: Residual data for Line 3 with reference map and bedrock type associated with the location of each gravity station.

Line 4

The residual gravity values for Line 4 **(Figure 21)** range by 0.760 mGal with a minimum value of 1.298 mGal and a maximum value of 2.058 mGal. The residual plot is much different than the Bouguer Anomaly plot. The residual plot shows a decrease from Station 1 to Station 5, an increase from Station 5 to Station 8, and a decrease from Station 8 to Station 10.

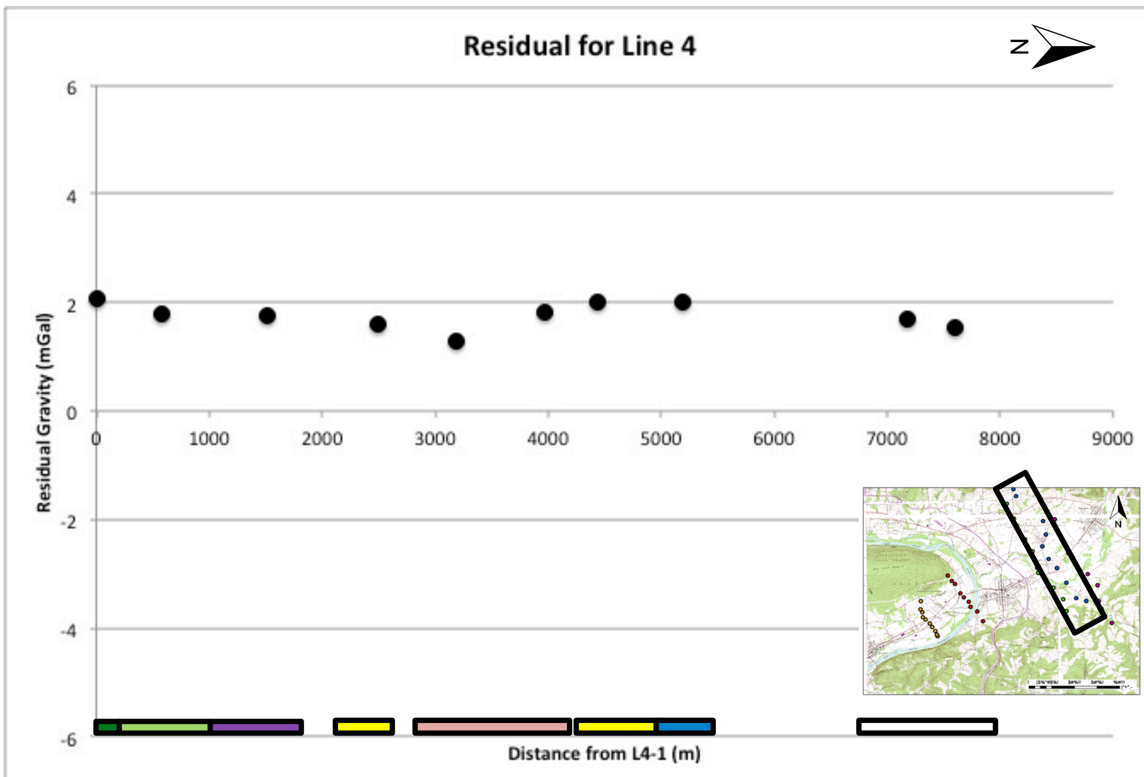

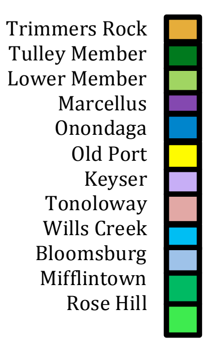

Figure 21: Residual data for Line 4 with reference map and bedrock type associated with the location of each gravity station.

Line 5

The residual gravity values for Line 5 **(Figure 22)** have a range of 1.366 mGal with a minimum value of 3.517 mGal and a maximum value of 4.883 mGal. The residual plot is much different than the Bouguer Anomaly plot. The residual plot shows a decrease from Station 1 to Station 5, and an increase from Station 5 to Station 10.

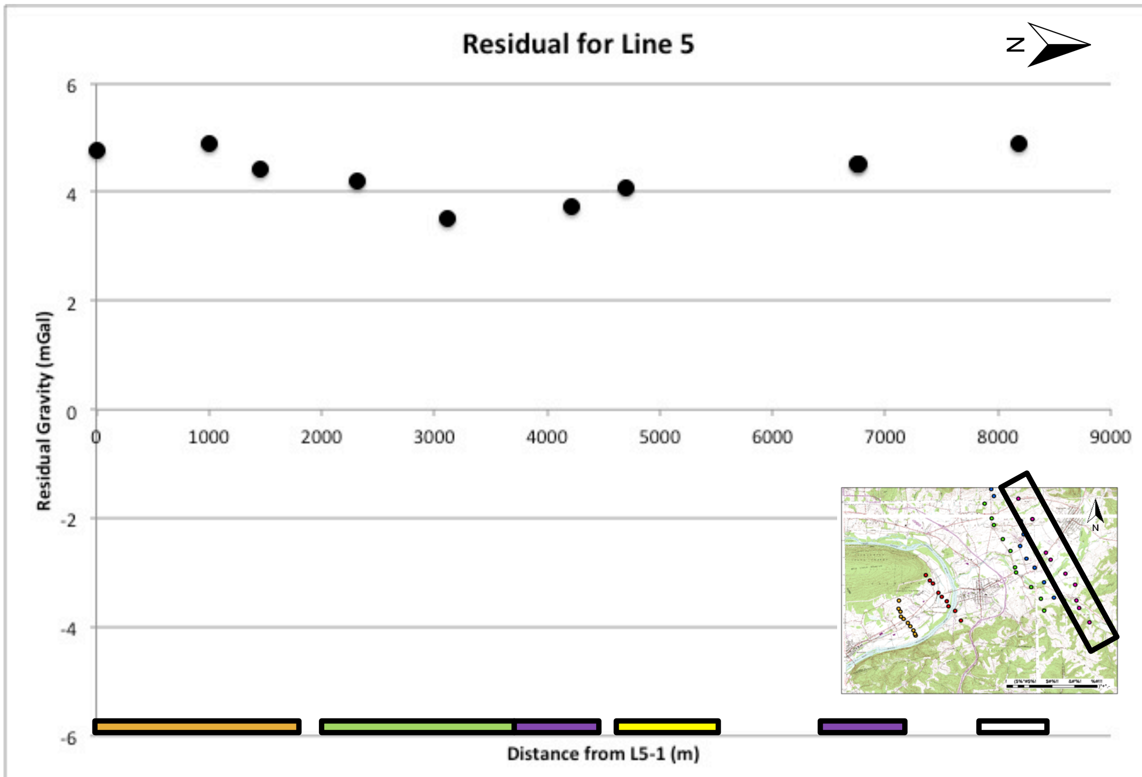

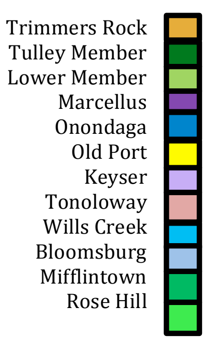

Figure 22: Residual data for Line 5 with reference map and bedrock type associated with the location of each gravity station.

Interpretations

Residual Anomaly Map

The Residual Anomaly map **(Figure 23)** was created through the interpolation of the post-processed gravity data over the extent of the study area (approximately 30 km^2). The data was interpolated using the kriging method. Kriging is a geostatistical interpolation method that estimates the value of a variable at an unmeasured location from surrounding observed points using a weighted sum. The weighting function assigns weights according to the proximity of surrounding points, giving closer points higher weights and farther points lower weights (Goovaerts, 1997).

This contour map shows an increasing residual anomaly from southwest to northeast. Areas where there are lower residual anomaly values indicate regions where lower density alluvium is thickest, and areas of increased values indicate regions where the alluvium is thinnest. Lines 1 and 2 (located in the southwest corner of map) correlate very well with saturated alluvium thickness map **(Figure 23)** showing the thickets alluvium to be located within the black box. The residual gravity data for Line 1 and Line 2 differ from the saturated alluvium thickness map in that the residual gravity data suggests that the thickest alluvium covers a larger area than shown by the dark red contour. Line 3 is also consistent with both the saturated alluvium thickness map and the well data map, showing a thickening of alluvium towards the middle of the line, a thinning of the alluvium, and then a thickening of the alluvium towards the northwest end of the line. The area inside the green box **(Figure 23)** shows that Point 4 from the residual data correlates well with the thickest section of alluvium as the saturated alluvium thickness map shows. Where the residual data and the alluvium thickness map differ is how thick the alluvium layer is. The residual data suggests that the alluvium in this area should be thinner than then that observed closer to Line 1 and Line 2, while the saturated alluvium thickness map shows that it is of similar thickness. Line 4 shows a thickening of alluvium towards the middle of the line, a thinning of alluvium towards the end of the line, and a thickening of the alluvium on the last points of the line in the northwest. The residual data for Line 4 also shows the area of thickest alluvium (green box in **Figure 23)** to be located where the saturated alluvium map indicates the thickest alluvium layer. As with Line 3, the Line 4 residual data suggest that the alluvium layer should be thinner than is suggested by the saturated alluvium thickness map. Line 5 shows a thickening of alluvium towards the middle of the line, with a steady thinning of alluvium towards the end of the line in the northwest. Unlike Line 3 and Line 4, Line 5 does not suggest that the thickest alluvium unit is located where the saturated alluvium thickness map indicates. Line 5 does however indicate that there should be a thinning of alluvium (green box on **Figure 23**) between Line 4 and Line 5. From the data on Line 5, the thickest section of alluvium occurs more closely to Muncy Creek than is indicated by the saturated alluvium thickness map (blue box on **Figure 23**).

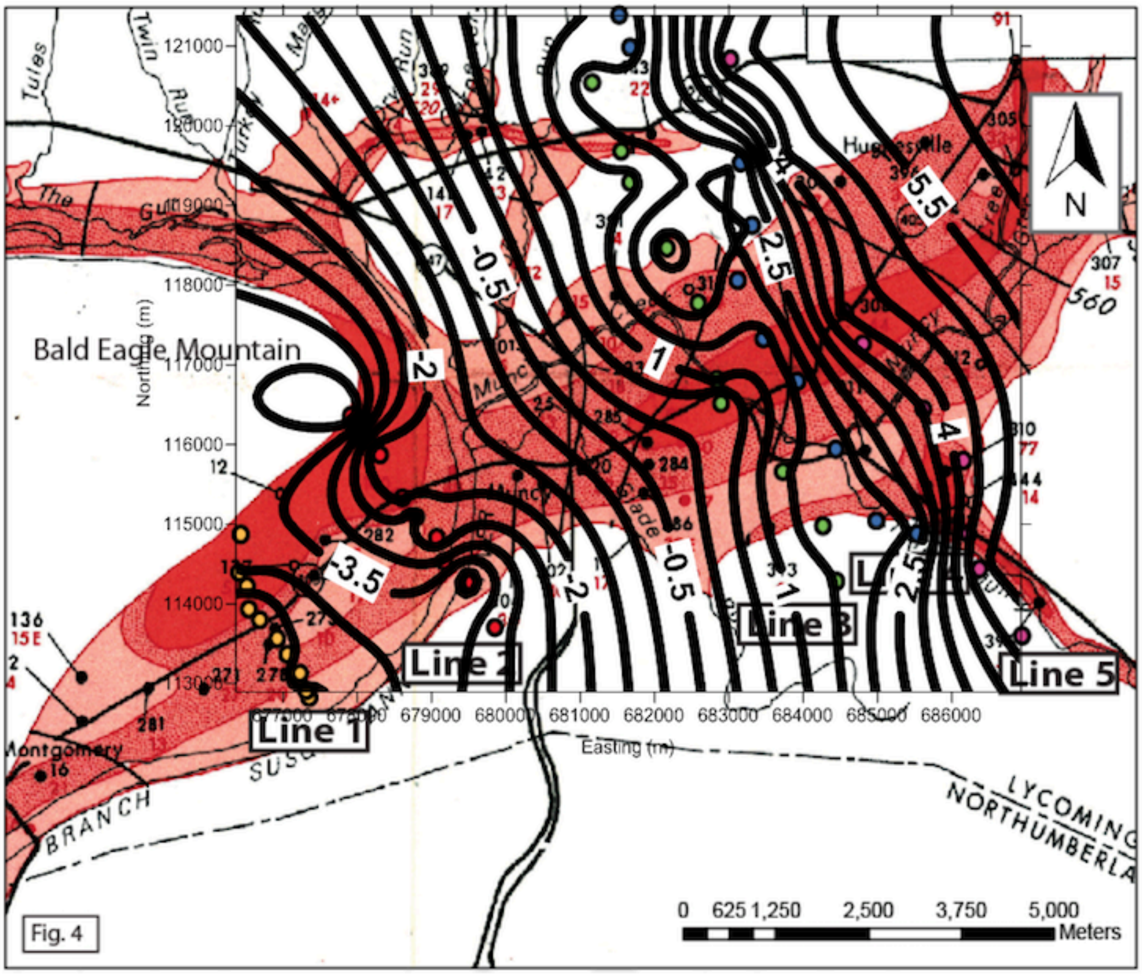

Figure 23: This graphic shows the interpolated residual anomaly contour map for the study area underlain by the saturated alluvium thickness map. See description of red, green and blue boxes in **Residual Anomaly Map** section.

2-D Semi-Infinite Slab Model

Model Description

The semi-infinite slab model was chosen as an initial model due to its similarity to the understood geometry of the alluvium. **Figure 24** shows what the semi-infinite slab method assumes the bedrock/alluvium geometry to look like. While this method will not be able to fully describe all of the nuances in the data, it is a good starting point for initial interpretations of the depth to bedrock and is a useful tool in our determination of an appropriate density contrast (used in the 3-D inversion model) for the Muncy study area. This model uses **Equation 2** to produce a gravity effect that is dependent upon the starting position of the slab, the density contrast between the slab and the overlying unit, and a thickness of the overlying unit.

$$\Delta g = 2G\Delta\rho t\left(\frac{\pi}{2} + \tan^{-1}\frac{x}{z}\right) \quad (2)$$

Where G is the universal gravitational constant ($6.67 \times 10^{-11} m^3 kg^{-1} s^{-2}$), $\Delta\rho$ is the density contrast, t is the thickness of the slab, x is the starting side of the slab, and h is the depth to the slab. The semi-infinite slab model assumes that the slab of material is rectangular and that it extends infinitely in the positive x (+x) direction. Due to these assumptions, only a partial amount of the data from a given line can be used at a time. In order to create a realistic model, the depth to bedrock value must be constrained by a known value of depth from a proximal area. For our model, local well data that reports the depth was used to bedrock to constrain the calculated depths, which also constrained the density contrast between the bedrock and the overlying alluvium **(Figure 24)**.

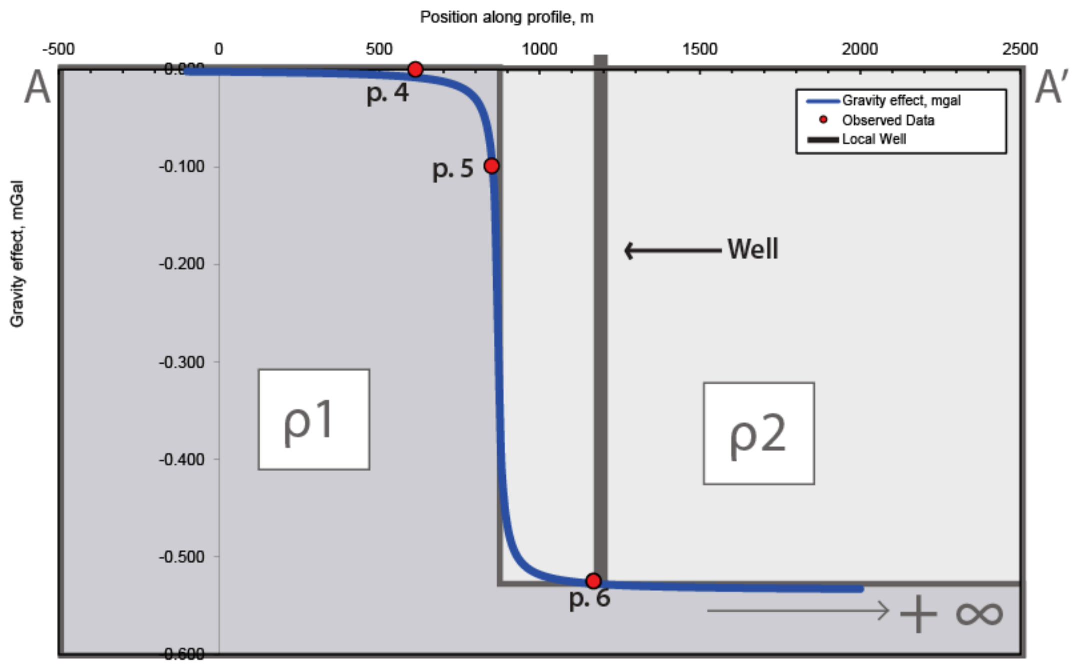

Figure 24: This figure shows the semi-infinite horizontal slab model for Line 1 (Points 4 through 6) overlying a simplified physical model of the bedrock and alluvium geometry.

Model Results

Line 1 – Points 4 through 6

Points 4 through 6 were chosen to analyze because they correspond to where the maximum thickness of alluvium is located. Based on well data in this area, the depth to bedrock should range from 0-20 meters. The density contrast needed to constrain the model to this depth is -0.7 g/cm^3.

Line 2 – Points 7 through 9

Points 7 through 9 were chosen to analyze due to their correlation with the increase in alluvium thickness. The well data from this area suggests that the depth to bedrock should range from 20-40 meters. The density contrast needed to constrain the model to this range is -0.8 g/cm^3.

Line 3 – Points 2 through 4

Points 2 through 4 were chosen due to the correlation with the maximum alluvium thickness. The depth to bedrock should range from 0-40 meters. The density contrast needed to constrain the model to this range is -2.00 g/cm^3. This density contrast is very large and unlikely realistic, thus it will not be used in our model. The density contrast is likely this large due to point 4 being a lower value than is reasonable. Comparing point 4 from Line 3 to the similar area of Line 4 indicates that point 4 from Line 3 is likely wrong. This error could arise due to seismic noise in the area, or other externalities.

Line 4 – Points 3 through 5

Points 3 through 5 were chosen for analysis due to their correspondence with the maximum alluvium thickness. The well data suggests that the depth to bedrock in this area should range from 20-40 meters. In order to constrain the model to this range, a density contrast of -0.8 g/cm^3 was used.

Line 5 – Points 3 through 5

Points 3 through 5 were chosen for analysis due to their correlation with the maximum alluvial thickness. The well data in this area suggests that the depth to bedrock should range from 40-60 meters. In order to constrain the model to this range, a density contrast of -0.8 g/cm^3 was used.

Study Area Density Contrast

Using the well data to constrain our semi-infinite slab model's calculation of depth to bedrock, a representative density contrast of -0.8 g/cm^3 for the study area (using Equation 2) was determined. This density contrast is realistic given the geology of the area. Our initial approximation of density contrast was -0.5 g/cm^3, based on a 2.7 g/cm^3 bedrock density and a 2.2 g/cm^3 saturated unconsolidated material density (based on 30% porosity). A plausible model to obtain a -0.8 g/cm^3 density contrast would be a 2.8 g/cm^3 bedrock density and a 2.0 g/cm^3 saturated unconsolidated material density (based on 40% porosity). This approximation of density contrast for the study area was used to generate our 3-D inversion model.

3-D Inversion Model

Inversion Theory

A Fourier transform can be used to express a gravity field in terms of amplitudes of individual sinusoidal shapes with different wavenumbers (Long et al., 2013). A continuous gravity field, Δg(x), can be equated to a sum of sine and cosine functions:

$$\Delta g(x) = a_0 + a_1 cos\frac{2\pi x}{L} + b_1 sin\frac{2\pi x}{L} + \cdots + a_n cos\frac{2\pi n x}{L} + b_n sin\frac{2\pi n x}{L} \quad (8)$$

Where *L* is the length of a line of data points, *n* is an integer from 0 to infinity, a_n and b_n are coefficients.

By considering the coefficients to be complex, the sum can be written in a more compact form:

$$\Delta g(x) = \sum_{k=1}^{\infty} a_k e^{i\frac{2\pi k x}{L}} \quad (9)$$

with the coefficients defined as:

$$a_k = \sum_{m=0}^{N-1} \Delta g_m e^{-i\frac{2\pi n m}{N}} \quad (10)$$

Where *N* is the number of gravity values at a separation of Δx=*L/N* (Long et al., 2013). For the descrete data the gravity data are expressed as the inverse Fourier transform as:

$$\Delta g_m = \Delta g(m\Delta x) = \frac{1}{N}\sum_{n=0}^{N=1} a_n e^{i\frac{2\pi n m}{N}} \quad (11)$$

This discrete Fourier transform can be calculated using the computationally efficient fast Fourier transform (FFT). The method used for the production of our 3-D model uses a FFT and is based on the equation:

$$F(\Delta g) = -2\pi G\rho e^{(-kz_0)} \sum_{n=1}^{\infty} \frac{k^{n-1}}{n!} F[h^n(x)] \quad (12)$$

Where $F(\Delta g)$ is the Fourier transform of the gravity anomaly, G is the gravitational constant, ρ is the density contrast across the interface, k is the wave number, h(x) is the depth to the interface (positive downwards) and z_0 is the mean depth of the horizontal interface (Parker, 1973).

This equation can be rearranged to solve for depth to the interface from the gravity anomaly profile through an iterative process (Oldenburg, 1974).

$$F[h(x)] = \frac{F[\Delta g(x)]e^{-kz_0}}{2\pi G\rho} - \sum_{n=2}^{\infty} \frac{k^{n-1}}{n!} F[h^n(x)] \quad (13)$$

The gravity data is then demeaned before the Fourier transform begins. Starting with h(x)=0, the inverse Fourier transform calculates the first approximation of the bedrock topography, h(x). This new value of h(x) is then used to approximate a new value of h(x). This process continues until a pre-set number of iterations is reached or when the difference between two successive approximations of the topography is lower than a defined value (Gómez-Ortiz et al., 2004).

To produce our 3-D model, a MATLAB function called 3dinver.m was used, which computes 2-D direct and inverse FFTs (Gómez-Ortiz et al., 2004). This function follows the Oldenburg (1974) procedure and is terminated when 10 iterations have been completed or when the RMS error falls below a user-defined limit (Gómez-Ortiz et al., 2004). This model produces four 3-D graphic outputs: (1) 3-D observed gravity data **(Figure 25)** (2) Topography of the bedrock-alluvium interface **(Figure 26)** (3) Bouguer Anomaly for the calculated bedrock-alluvium interface **(Figure 27)** and (4) The difference between the input gravity data and the calculated gravity data **(Figure 28)**.

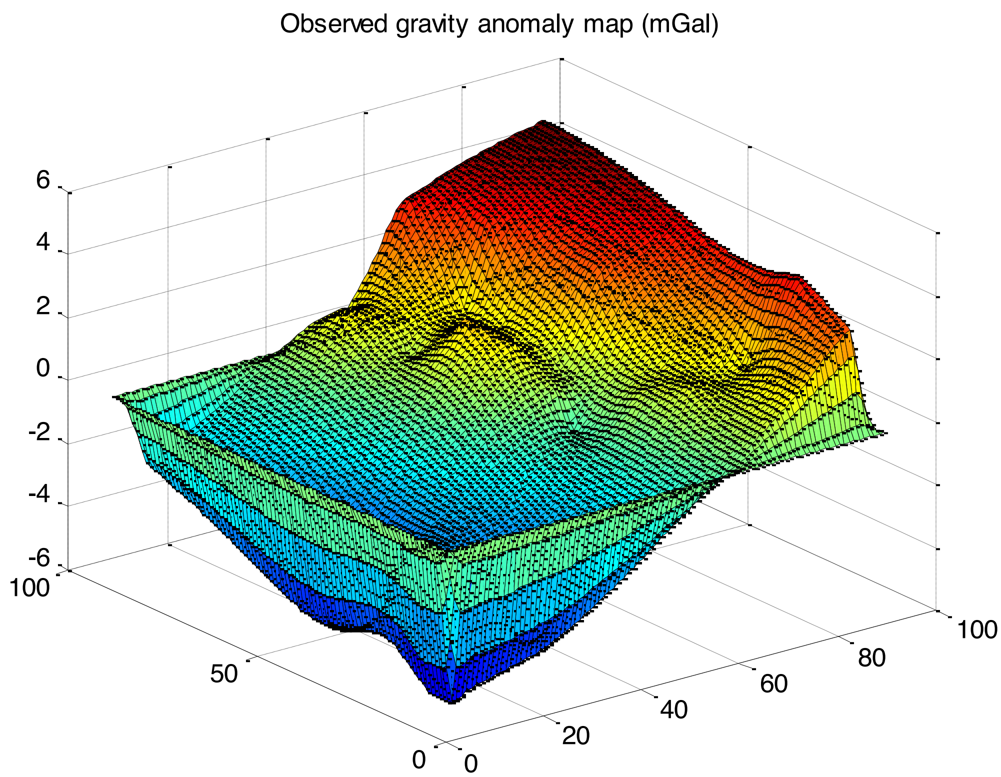

Figure 25: This graphic shows the 3-D visualization of the observed gravity data.

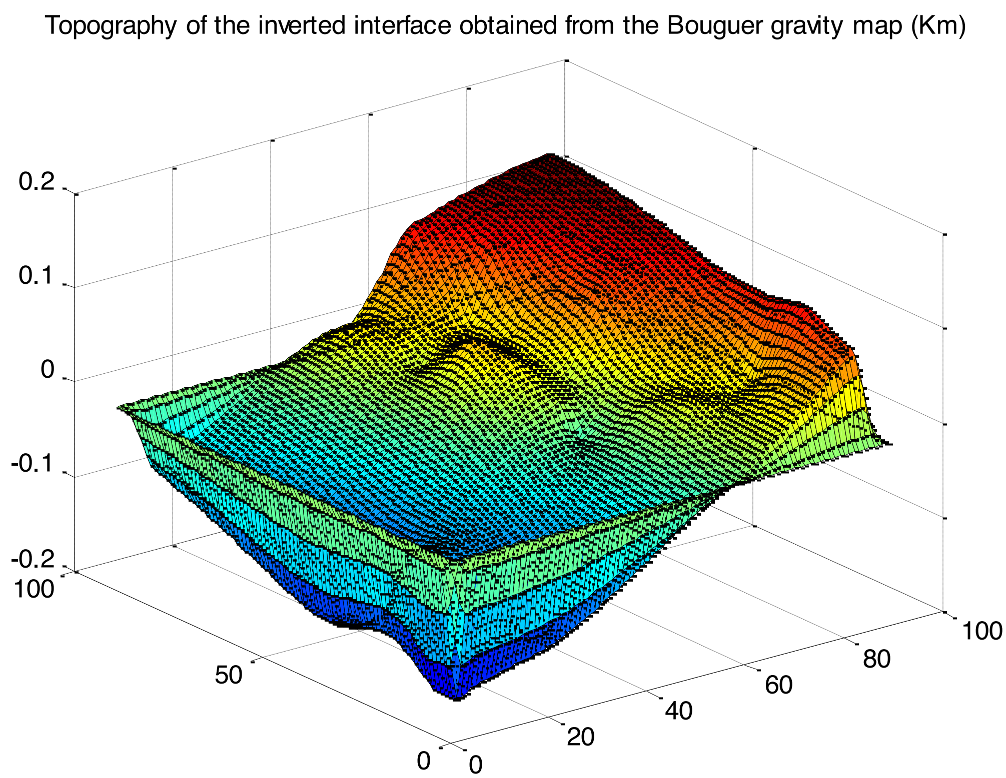

Figure 26: This graphic shows the calculated topography of the bedrock-alluvium interface.

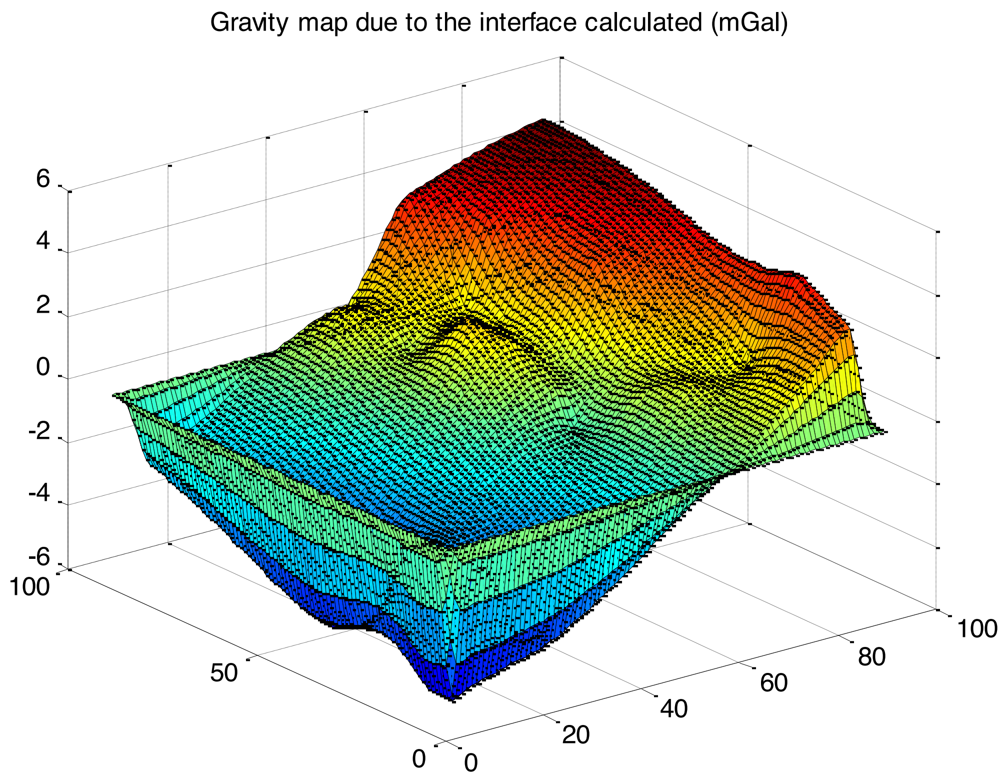

Figure 27: This graphic shows the calculated gravity anomaly caused by the bedrock-alluvium interface from Figure 26.

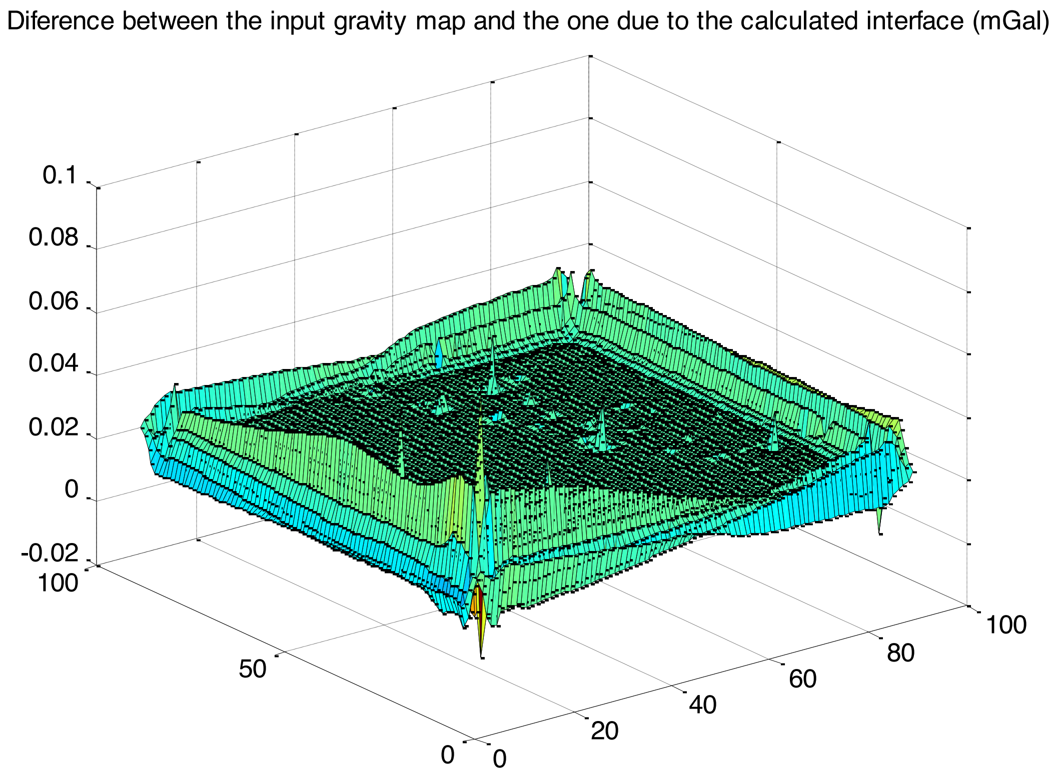

Figure 28: This graphic shows the difference between the observed gravity anomaly and the calculated gravity anomaly from the bedrock-alluvium interface.

Inversion Interpretations

For our inversion model we used -0.8 g/cm^3 (determined from the semi-infinite slab method) for the density contrast between the bedrock and alluvium. **Figure 26** shows a maximum thickness of alluvium occurring in the southwest corner of the study area (approximately 160 meters thick), with continuously thinning alluvium towards the northeast of the study area (approximately 10 meters thick). The red areas of the graphic (the northeast-southeast boarder) are likely artifacts in the data associated with the kriging process. The 3-D aspect of these graphics makes it difficult to include surface geographic features for comparison. In order to use the 3-D image of bedrock topography for comparison with surface geographic features, the calculated topography matrix from MATLAB was brought into Surfer and plotted as a 2-D contour map. **Figure 29** is a 2-D version of the 3-D topography model, with the gravity stations overlain. The lowest topography in the southwest and the highest topography in the northwest, suggesting that the thickest alluvium in the valley is located in the southwest.

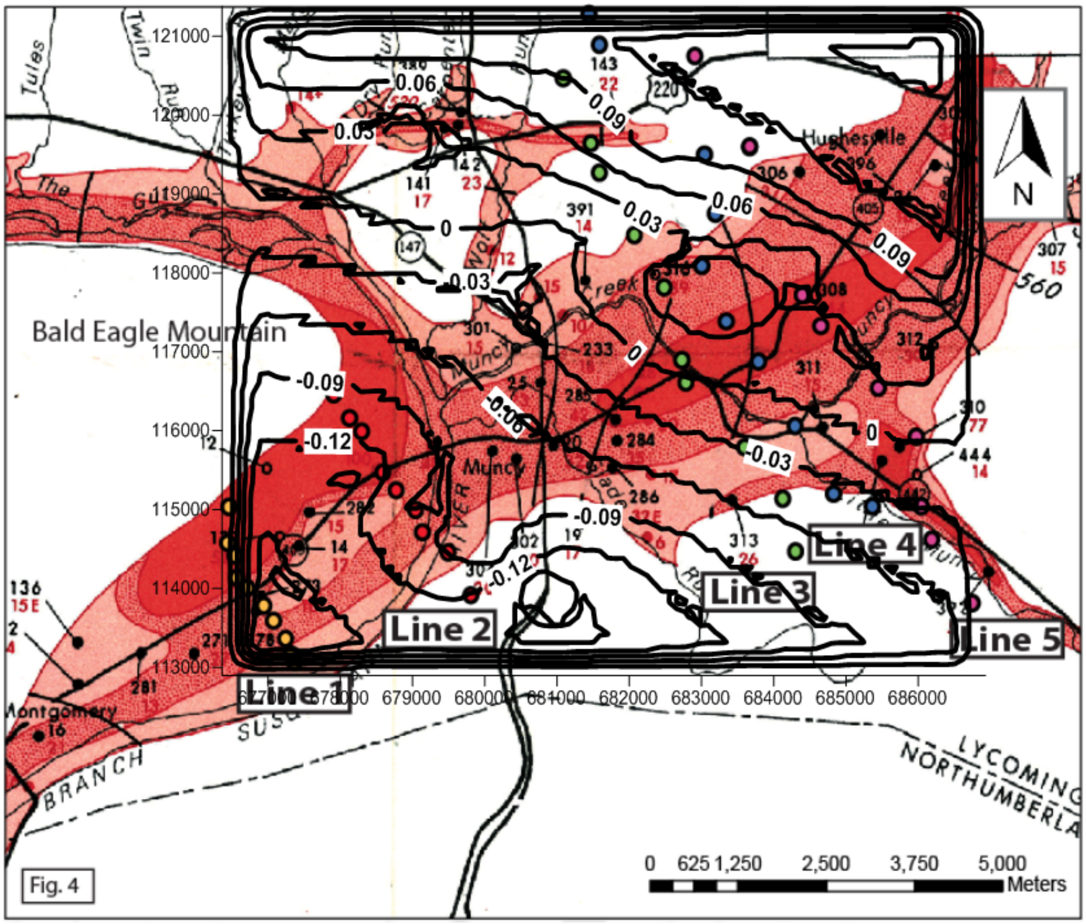

Figure 29: 2-D contour map showing the bedrock topography over the study area. This 2-D contour map is overlain on the saturated alluvium thickness map. Note: there is some correspondence in the bedrock topography data and the thick saturated alluvium in the southeast.

Discussion

Looking at the residual gravity data for Line 1 and Line 2 **(Figures 18-19)**, it is possible to observe the channel migration of the WBSR. Due to the geometry of the river at this location (The Great Bend), the channel migrated from West to East, leaving behind terraces as evidence of historic channel locations and down-cutting through sediment. **Figure 30 (Engel et al., 1996)** shows a surficial geology cross-section of "The Great Bend" area near Line 1 and Line 2. This figure shows a thickening of alluvium towards the middle of the lines (northwest direction), a gradual thinning of alluvium from the middle to the end with a possible re-thickening of alluvium at the end of the line (Engel et al., 1996). The data from Line 1 do not reflect the understanding put forth by Engel (1996). **Figure 31** illustrates an estimate of the gravity change over the cross-sectional area from **Figure 30** using **Equation 2** with ρ=-0.8 g/cm^3, z=the alluvium thickness from Engel (1996), and G is the universal gravitational constant. According to the Engel (1996) model, the gravity anomaly should not change much since the thickness of alluvium does not vary much. For the 5 points that were chosen to make this estimated gravity profile **(Figure 31)**, the anomaly varies by 0.002 mGal, while the residual data for Line 1 vary by 1.404 mGal. The residual data from the same area that Engel (1996) studied show a much different picture of the subsurface, indicting that the Engel (1996) model may underestimate the changes in alluvium thickness in this area.

Line 1 has the thickest alluvium located to the North of the modern channel, with a thinning pattern as the line approaches Bald Eagle Mountain. Line 2 does not follow

Engel (1996) exactly, but it does show a thickening of alluvium towards to location of the modern channel of the WBSR from the south, a thinning of alluvium to the north of the modern channel WBSR and then a re-thickening of alluvium as the line approaches Bald Eagle Mountain. Line 3 shows a thickening of alluvium towards the modern channel of Muncy Creek from the south, a thinning of alluvium to the north of the modern channel of Muncy Creek, a slight thickening at Point 8, and a thinning to the north of Point 8. The thickest alluvium from Line 4 does not correspond with the location of the modern channel of Muncy Creek, but rather to the north of he channel at Point 5. From Point 5, the alluvium shows a thinning trend to Point 7 and a slight rethickening to Point 10. Line 5 shows a thickening of alluvium with a maximum depth being located between Point 5 and Point 6 which are to the south and north of the modern channel of Muncy Creek respectively. From the modern channel, there is a thinning pattern of alluvium to the north that continues until Point 10.

The gravity profiles for Lines 1 through 5 show an increasing gravity anomaly towards the northeast, suggesting that the alluvium layer thins in the northeast direction, with the thickest alluvium layer located in the southwest. The geologic structure of the valley **(Figure 2)** shows that the valley reaches a terminus as it approaches the bedrock ridges that surround this valley. Since the low topography of the valley transitions into the high topography of the ridges, the bedrock elevation must increase towards the northeast thus causing the alluvium to thin. This geometry is consistent with the increase in the gravity anomaly seen from Line 1 to Line 5.

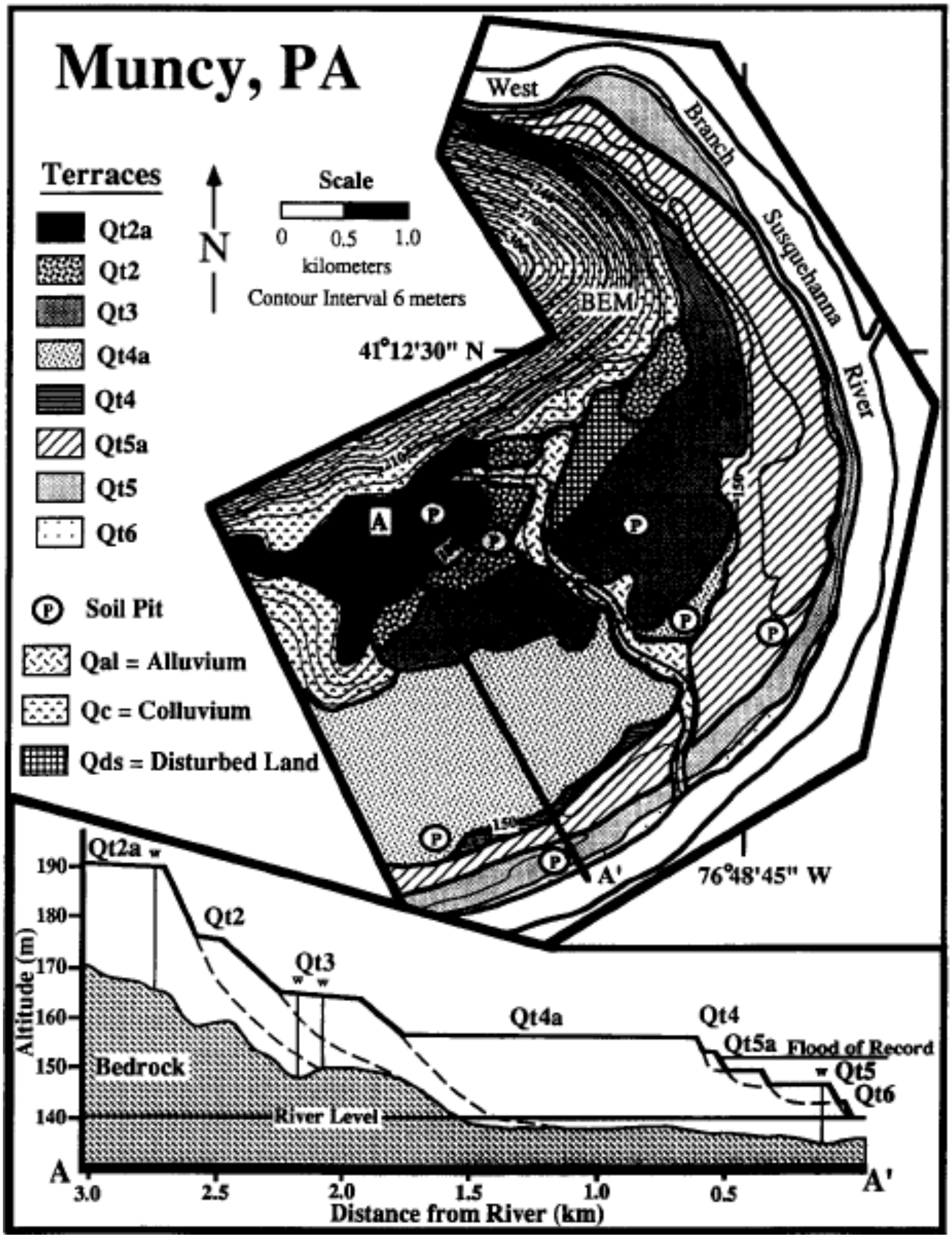

Figure 30: Topographic map, surficial geology, and cross section of Muncy, PA showing distribution of terraces and soil pit locations. (Engel et al., 1996).

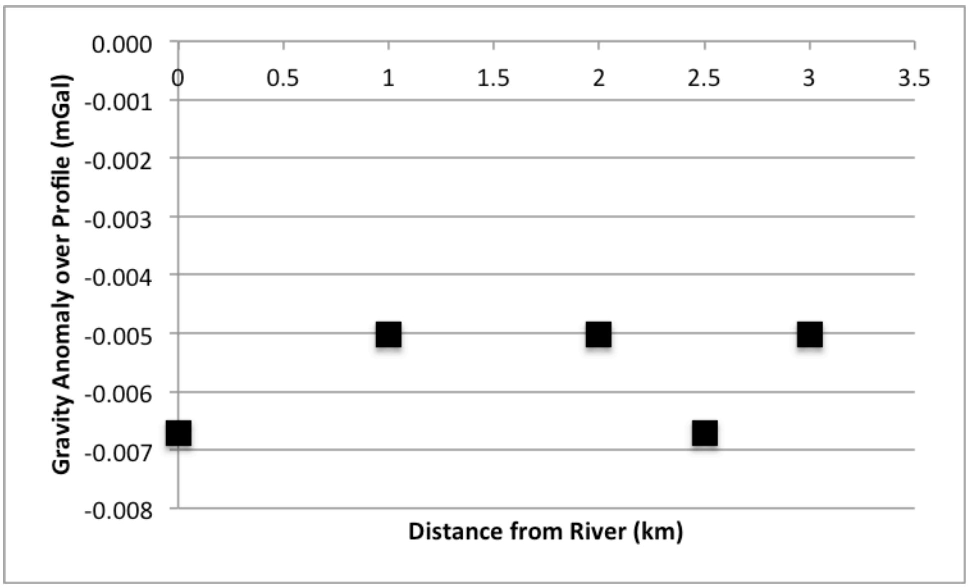

Figure 31: The estimated gravity anomaly over the cross-sectional area proposed by Engel et al., 1996.

Future Work

Future projects in this location should be focused on obtaining more gravity readings, using the established base stations from this project. Possible areas of interest should include a transect that runs perpendicular through all the lines for the length of the valley, increased data density in the middle of Line 3 through 5, and further study of the area around Line 2 and Line 3. By increasing our data density the bedrock-alluvium topography model will become stronger, allowing for a greater understanding of the Muncy area as a whole. With the increased data set, it may also be of interest to look into the use of different modeling software with the goal of comparing the predicted bedrock-alluvium topography.

Conclusions

Using five micro-gravity survey lines in conjuncture with local well logs from the area surrounding Muncy, PA, along the WBSR, the bedrock-alluvium interface was detected and depth to bedrock was able to be determined. The data show an increase in the gravity anomaly from southeast to northeast, suggesting that the thickest alluvium (approximately 160 meters) is located to the southeast of Muncy (Line 1), with a thinning pattern toward the northeast (Line 5). Comparing the Line 5 residual data to the saturated alluvium thickness map shows that the thickest alluvium in this area actually occurs closer to Muncy Creek than is indicated by the saturated alluvium thickness map. To account for the thickest alluvium immediately proximal to Bald Eagle Mountain in the southeast, it is possible that a glacial lobe during the Pleistocene glaciation traveled down Muncy Creek Valley to a point where the WBSR would become constrained against the bedrock ridge. While constrained here, the WBSR likely deeply downcut and deposited the sediment layer that we see today. It is also likely that Muncy Creek had a role in the deposition of the thickest sediment layer suggesting that both glacial and fluvial processes are responsible for the bedrock-alluvium topography we see today. Subsequent flooding and meandering caused the WBSR to move to its modern location to the east of the thickest alluvium. The geologic structure of the valley is consistent with a thinning of the alluvium towards the northeast because the low topography of the valley must transition into the high topography of the surrounding ridges, thus thinning the alluvium. This study suggests that the gravity method together with local well data may be used to determine the depth to bedrock over the extent of alluvial valleys, offering an efficient, low-cost and non-invasive technique to explore the subsurface and supplement existing well data.

Bibliography

Ander, M. E., T. Summers, and M. E. Gruchalla, 1999, LaCoste & Romberg gravity meter: System analysis and instrumental errors: Geophysics, 64, no. 6, P. 1708-1719.

Bohidar, R. N., Sullivan, J. P. and Hermance, J. F., 2001, Delineating Depth to Bedrock Beneath Shallow Unconfined Aquifers: A Gravity Transect Across the Palmer River Basin. Ground Water, 39: 729–736. doi: 10.1111/j.1745-6584.2001.tb02363.x

Engel, S. A., Gardner, T. W., Ciolkosz, E. J., 1996, Quaternary soil chronosequences on terraces of the Susquehanna River, Pennsylvania, *Geomorphology* 17 (1996), 273-294.

Faill, R. T., 1979, Geology and mineral resources of the Montoursville South and Muncy quadrangles and part of the Hughesville quadrangle, Lycoming, Northumberland, and Montour Counties, Pennsylvania: Pennsylvania Geological Survey Atlas 144ab.

Fetter, C.W., 2000, Applied hydrogeology: Prentice Hall; 4th edition.

Gómez-Ortiz, D., Agarwal, B.N.P., 2004, 3DINVER.M: a MATLAB program to invert the gravity over a 3D horizontal density interface by Parker-Oldenburg's algorithm, *Computers & Geosciences* 31 (2005), 513-520.

Goovaetrts, P., 1997, Geostatistics for Natural Resource Evaluation: Oxford University Press.

Hayes, Benjamin R. and Newlin, Jessica T., 2012. Use of Hydro-Acoustics in Undergraduate Teaching and Research: Measuring Flow Hydraulics, River Bedforms, and Sediment Discharge in the Susquehanna Watershed, North-Central Pennsylvania, Joint U.S. Geological Survey and Consortium of Universities for the Advancement of Hydrolgic Sciences Workshop on Sediment-Hydroacoustics, National ConservationTraining Center, Shepherdstown, WV, March 5-7.

Kochel, R.C., Nickelsen, R.P., Eaton, L.S., 2009, Catastrophic middle Pleistocene jökulhlaups in the upper Susquehanna River: Distinctive landforms from breakout floods in the central Appalachians, *Geomorphology*, v. 110, p. 80-95

Lloyd, O. B., Jr., and L. D. Carswell, 1981, Groundwater resources of the Williamsport region, Lycoming County, Pennsylvania: Pennsylvania Geologic Survey Water Resources Report W51

Long, T.L., Kaufman, R.D., 2013, Acquisition and Analysis of Terrestrial Gravity Data: Cambridge University Press.

Micro-g LaCoste, 2002, Graviton EG instrument manual.

Newlin, Jessica T., Hayes, Benjamin R., and Yee, Kayla*, 2013. Morphologic Investigation of the West Branch of the Susquehanna River in North-Central Pennsylvania, World Environmental and Water Resources Congress, American Society of Civil Engineers (ASCE), Cincinnati, OH, May 19-23, 2013, p. 87-94.

Oldenburg, D.W., 1974. The inversion and interpretation of gravity anomalies. Geophysics 39 (4), 526–536.

Parker, R.L., 1973. The rapid calculation of potential anomalies. Geophysical Journal of the Royal Astronomical Society 31, 447–455.

Parrish, J. B., and Lavin, P. M., 1982, Tectonic model for kimberlite emplacement, in the Appalachian Plateau of Pennsylvania: Geology, v. 16, p. 344-347.

Ramage, M.J., Gardner, W.T., and Sasowsky, D.I., 1998, Early Pleistocene Glacial Lake Lesley, West Branch Susquehanna River valley, central Pennsylvania. *Geomorphology.* v. 22, p. 19-37.

Sevon, Bill., 1993, River on a Rampage. *Pennsylvania Geology*. v.24, no. 2, p. 6.

Sharma, P.V., 1986, Geophysical methods in geology: Elsevier Science Ltd; 2nd edition.

Telford, W. M., L. P. Geldart, and R. E. Sheriff, 1990, Applied geophysics: Cambridge University Press.

Trimble, 2013, Trimble R8 GNSS System manual

APPENDIX A

Name	GPS Point	Northing (m)	Easting (m)	Elevation (m)	Drift Corrected Gravity	Free-Air Correction	Latitude Correction	Bouguer Correction	All Corrections Appl.	Δg (mgal)
L1-1	126	112893.651	677310.458	144.335	3839.414769	44.541781	0	16.34030969	3867.616241	3867.61624
L1-2	125	112986.227	677266.844	146.728	3839.279225	45.2802608	0.001354445	16.61122361	3867.949616	3867.94826
L1-3	124	113191.344	677188.85	149.783	3838.511224	46.2230338	0.004355415	16.95708321	3867.78153	3867.77717
L1-4	123	113429.891	677013.896	152.769	3837.573275	47.1445134	0.007845407	17.29513126	3867.430503	3867.42266
L1-5	122	113629.09	676883.068	154.566	3837.123244	47.6990676	0.010759621	17.49857143	3867.3345	3867.32374
L1-6	121	113854.65	676646.158	154.134	3836.782034	47.5657524	0.014059319	17.44966427	3866.912182	3866.89812
L1-7	128	113990.713	676496.819	154.417	3836.752835	47.6530862	0.016049664	17.48170299	3866.940268	3866.92422
L1-8	129	114281.608	676467.902	166.601	3834.978263	51.4130686	0.02030457	18.86106581	3867.55057	3867.53027
L1-9	130	114450.569	676363.319	168.525	3834.673481	52.006815	0.022775705	19.07888378	3867.624188	3867.60141
L1-10	131	114925.574	676384.825	189.154	3830.917922	58.3729244	0.029721674	21.41431349	3867.906255	3867.87653

Name	GPS Point	Northing (m)	Easting (m)	Elevation (m)	Drift Corrected Gravity	Free-Air Correction	Latitude Correction	Bouguer Correction	All Corrections Appl.	Δg (mgal)
L2-2	104	113766.597	679820.818	173.988	3835.12806	53.6926968	0	19.69735547	3869.123401	3869.1234
L2-3BASE	102	114326.847	679498.506	146.578	3839.142514	45.2339708	0.008196672	16.59424196	3867.79044	3867.78224
L2-4	109	114587.315	679124.549	147.361	3840.216506	45.4756046	0.012007184	16.68288617	3869.021232	3869.00922
L2-5	108	114884.793	679033.783	149.923	3840.506726	46.2662378	0.016358806	16.97293275	3869.816389	3869.80003
L2-6	107	115135.630	678759.664	150.734	3839.536123	46.5165124	0.020027785	17.06474687	3869.007917	3868.98789
L2-7-4BASE	105	115370.688	678572.715	150.987	3840.203939	46.5945882	0.023465596	17.09338926	3869.728603	3869.70514
L2-8-2	111	115907.304	678265.864	165.695	3837.230769	51.133477	0.031312128	18.75849665	3869.637061	3869.60575
L2-9	113	116082.721	678094.997	168.384	3835.639112	51.9633024	0.03387652	19.06292102	3868.57337	3868.53949
L2-10	112	116397.486	677875.725	186.338	3830.136153	57.5039068	0.038477151	21.09551132	3866.583026	3866.54455

Name	GPS Point	Northing (m)	Easting (m)	Elevation (m)	Drift Corrected Data	Free-Air Correction	Latitude Correction	Bouguer Correction	All Corrections Appl.	Δg (mgal)
L3-1	134	114339.043	684428.548	263.096	3822.441652	81.1914256	0	29.78536126	3873.847716	3873.84772
L3-2-	133	115034.421	684242.699	181.578	3838.436922	56.0349708	0.010173552	20.55662696	3873.92544	3873.91527
L3-3-BASE	132	115699.09	683704.114	162.735	3841.334688	50.220021	0.019896354	18.42339209	3873.151213	3873.13132
L3-4-BASE2	135	116554.47	682873.82	158.406	3840.325445	48.8840916	0.032404487	17.93330167	3871.30864	3871.27624
L3-5	136	116847.847	682808.064	153.846	3842.254384	47.4768756	0.036692885	17.41705951	3872.350893	3872.3142
L3-6	137	117802.472	682560.679	163.547	3841.087002	50.4706042	0.050639268	18.51531942	3873.092926	3873.04229
L3-7	138	118484.522	682139.93	164.308	3841.111683	50.7054488	0.060594592	18.60147299	3873.276254	3873.21566
L3-8	144	119306.164	681644.337	166.049	3838.870219	51.2427214	0.072575136	18.79857334	3871.386942	3871.31437
L3-9	147	119689.062	681521.834	162.983	3839.942637	50.2965538	0.078152983	18.45146841	3871.865875	3871.78772
L3-10	146	120541.712	681123.76	188.609	3834.952944	58.2047374	0.090560164	21.3526135	3871.895628	3871.80507

Name	GPS Point	Northing (m)	Easting (m)	Elevation (m)	Drift Corrected Date	Free-Air Correction	Latitude Correction	Bouguer Correction	All Corrections Appl.	(Δg)mgal)
L4-1-	160	114933.797	685512.843	168.546	3841.445669	52.0132956	0	19.08126121	3874.377704	3874.3777
L4-2	165	115095.104	684960.465	171.639	3840.336569	52.9677954	0.00236002	19.43142283	3873.875302	3873.87294
L4-3	142	115980.92	684421.183	156.506	3842.9067	48.2977516	0.015319161	17.71820077	3873.50157	3873.48625
L4-4-BASE1	140	116828.195	683894.336	156.082	3842.427962	48.1669052	0.027710856	17.6701993	3872.952379	3872.92467
L4-5-BASE3	141	117351.078	683437.655	161.945	3840.701549	49.976227	0.035355165	18.3339554	3872.379176	3872.34382
L4-6	175	118083.599	683092.157	162.954	3840.708251	50.2876044	0.046058855	18.44818529	3872.593729	3872.54767
L4-7	180	118766.359	683289.143	181.531	3837.095423	56.0204666	0.056028245	20.55130604	3872.620612	3872.56458
L4-8	185	119542.141	683131.6	189.203	3835.293169	58.3880458	0.067345531	21.41986083	3872.3287	3872.26135
L4-9	191	120984.782	681642.998	187.729	3834.44904	57.9331694	0.088354441	21.25298782	3871.217576	3871.12922
L4-10	190	121383.29	681497.209	196.573	3832.408273	60.6624278	0.094147919	22.2542259	3870.910623	3870.81648

Name	GPS Point	Northing (m)	Easting (m)	Elevation (m)	Drift Correct Data	Free-Air Correction	Latitude Correction	Bouguer Correction	All Corrections Appl.	(Δg)mgal)
L5-1	225	113665.291	686931.807	209.619	3836.137567	64.6884234	0	23.73117661	3877.094814	3877.09481
L5-2	230	114493.99	686361.788	166.015	3844.363333	51.232229	0.012123938	18.79472417	3876.812962	3876.80084
L5-3	220	114932.588	686208.875	165.116	3843.904741	50.9547976	0.018539743	18.69294748	3876.185131	3876.16659
L5-4	215	115845.018	686135.761	177.536	3840.90079	54.7876096	0.031882583	20.0990281	3875.621254	3875.58937
L5-5-BASE	200	116483.464	685598.674	166.588	3842.040742	51.4090568	0.041213932	18.85959407	3874.631419	3874.5902
L5-6	205	117293.134	684783.366	159.939	3843.121708	49.3571754	0.053039841	18.10685413	3874.425069	3874.37203
L5-7	210	117702.11	684518.039	164.779	3842.313875	50.8507994	0.059009145	18.65479537	3874.568888	3874.50988
L5-8-BASE2	300	119640.892	683774.398	185.602	3837.860808	57.2767772	0.087257993	21.01218802	3874.212655	3874.1254
L5-9	305	119644.778	683773.091	185.818	3837.830763	57.3434348	0.087314518	21.0366416	3874.224871	3874.13756
L5-10	310	120837.288	682998.309	204.315	3834.006957	63.051609	0.10463904	23.13070547	3874.032499	3873.92786

APPENDIX B

Longitude	Latitude	Depth to Bedrock (m)
-76.8667	41.2333	213.0552
-76.8667	41.1500	60.96
-76.8667	41.1667	121.92
-76.8667	41.2333	96.9264
-76.8500	41.1667	76.2
-76.8500	41.1833	27.432
-76.8500	41.1667	138.684
-76.8500	41.1667	61.8744
-76.8500	41.2333	60.96
-76.8500	41.2500	42.672
-76.8500	41.2300	54.864
-76.8500	41.2300	54.864
-76.8500	41.2300	48.768
-76.8492	41.1648	6.096
-76.8472	41.1906	23.1648
-76.8367	41.1758	11.2776
-76.8333	41.1667	99.6696
-76.8333	41.1667	92.0496
-76.8333	41.2333	65.532
-76.8333	41.2333	64.6176
-76.8333	41.1500	33.528
-76.8325	41.1953	17.6784
-76.8322	41.1961	14.0208
-76.8314	41.2392	48.768
-76.8314	41.2392	3.048
-76.8300	41.1800	22.86
-76.8200	41.2300	91.44
-76.8200	41.2300	91.44
-76.8197	41.2478	5.4864
-76.8186	41.2378	12.192
-76.8178	41.1794	4.2672
-76.8175	41.2342	1.8288
-76.8167	41.2000	21.6408
-76.8167	41.2000	9.144
-76.8167	41.1833	99.06
-76.8167	41.1833	33.2232
-76.8167	41.1833	31.3944
-76.8167	41.1833	27.432
-76.8167	41.1833	19.2024
-76.8167	41.1833	42.9768
-76.8167	41.1833	76.2
-76.8167	41.2333	45.72

-76.8125	41.2367	18.5928
-76.8117	41.2453	9.144
-76.8106	41.1848	6.096
-76.8097	41.2453	4.572
-76.8064	41.2769	4.2672
-76.8031	41.1733	3.048
-76.8031	41.2489	7.62
-76.8017	41.2206	6.4008
-76.8000	41.2333	10.668
-76.8000	41.2167	121.92
-76.8000	41.2500	152.4
-76.7998	41.1904	5.7912
-76.7980	41.1944	12.4968
-76.7980	41.1908	3.6576
-76.7975	41.2506	7.0104
-76.7923	41.2277	14.3256
-76.7908	41.2084	15.5448
-76.7903	41.2439	8.5344
-76.7897	41.1935	3.9624
-76.7884	41.2165	11.5824
-76.7833	41.2000	92.0496
-76.7833	41.2000	24.384
-76.7833	41.2000	42.672
-76.7833	41.2000	24.384
-76.7833	41.2000	42.672
-76.7833	41.2167	8.5344
-76.7833	41.2167	8.5344
-76.7833	41.2167	65.532
-76.7833	41.2167	9.4488
-76.7833	41.2000	60.96
-76.7833	41.2167	11.5824
-76.7833	41.2000	41.148
-76.7833	41.2000	53.34
-76.7833	41.2000	44.196
-76.7800	41.2300	36.576
-76.7800	41.2500	53.34
-76.7776	41.2198	5.1816
-76.7769	41.1975	6.7056
-76.7757	41.1980	9.144
-76.7740	41.1976	9.144
-76.7733	41.2689	3.048
-76.7711	41.2394	15.24
-76.7700	41.2200	33.528
-76.7700	41.2200	36.576
-76.7700	41.2200	28.6512

-76.7667	41.1833	6.7056
-76.7667	41.2000	30.48
-76.7667	41.2000	33.8328
-76.7667	41.2000	22.86
-76.7667	41.2000	31.0896
-76.7667	41.2333	24.9936
-76.7667	41.2167	24.0792
-76.7667	41.2333	51.816
-76.7667	41.1833	15.24
-76.7667	41.2500	60.96
-76.7633	41.2106	25.908
-76.7617	41.2494	12.4968
-76.7602	41.2035	7.62
-76.7600	41.2267	16.4592
-76.7586	41.2030	12.192
-76.7564	41.2022	9.144
-76.7500	41.2167	36.576
-76.7500	41.2167	15.8496
-76.7500	41.2333	32.004
-76.7500	41.2167	30.48
-76.7500	41.1800	91.44
-76.7489	41.1994	5.4864
-76.7481	41.2183	11.2776
-76.7433	41.2064	30.48
-76.7389	41.1861	2.4384
-76.7386	41.2053	22.2504
-76.7333	41.2333	17.3736
-76.7333	41.2167	28.0416
-76.7333	41.2000	27.432
-76.7333	41.2500	134.112
-76.7333	41.2333	16.764
-76.7328	41.2022	22.2504
-76.7300	41.2000	83.82
-76.7300	41.2000	60.96
-76.7300	41.2000	29.8704
-76.7200	41.2200	53.34
-76.7200	41.2000	59.436
-76.7167	41.2500	29.2608
-76.7167	41.2500	14.6304
-76.7167	41.2500	14.9352
-76.7167	41.2000	45.72
-76.7167	41.2500	45.1104
-76.7167	41.2000	39.0144
-76.7167	41.2000	60.96
-76.7167	41.2000	30.48

-76.7000	41.2167	15.24
-76.7000	41.2167	45.72
-76.7000	41.2167	109.728